A multi-omics study of diagnostic markers and the unique inflammatory tumor micro-environment involved in tuberous sclerosis complex-related renal angiomyolipoma

ZHAN WANG[1*], XIAOYAN LIU[2*], WENDA WANG[1], JING WEI[3], SAMUEL SEERY[4,5], JIYU XU[2], HAIDAN SUN[2], YUNCUI YU[3], YANG ZHAO[1], XU WANG[1], ZHANGCHENG LIAO[1], YANAN LI[1], WEI SUN[2], LULU JIA[3] and YUSHI ZHANG[1]

[1]Department of Urology, Peking Union Medical College Hospital, Chinese Academy of Medical Science and Peking Union Medical College; [2]Core Facility of Instrument, Institution of Basic Medical Sciences, Chinese Academy of Medical Sciences, School of Basic Medical College, Beijing 100730; [3]Clinical Research Center, National Center for Children's Health, Beijing Children's Hospital, Capital Medical University, Beijing 100045; [4]School of Humanities and Social Sciences, Chinese Academy of Medical Sciences and Peking Union Medical College, Beijing 100730, P.R. China; [5]Faculty of Health and Medicine, Division of Health Research, Lancaster University, Lancaster LA1 4YW, UK

Received July 8, 2022; Accepted August 23, 2022

DOI: 10.3892/ijo.2022.5422

Abstract. Tuberous sclerosis complex (TSC) is a rare disease that threatens multiple organs in the human body. TSC-associated renal angiomyolipoma (TSC-RAML) has potentially life-threatening complications and a generally poor prognosis. The present study aimed to find plasma proteomic diagnostics and disease-associated markers, and explore the tumor microenvironment using multi-omics. To achieve this goal, the plasma proteomics as well as tissue proteomics, bulk and single-cell RNA transcriptome from patients with TSC-RAML were examined and analyzed. The results suggested that plasma proteins such as MMP9 and C-C motif chemokine ligand 5 were able to differentiate TSC-RAML from sporadic angiomyolipoma and renal cyst. A correlation analysis revealed that plasma proteomics were associated with lymphangioleiomyomatosis, TSC-RAML grading and whole-body disease burden. Tissue proteomics of participants with TSC-RAML revealed disturbed small molecule catabolic process, mitochondrial matrix component and actin binding function. Bulk and single-cell RNA sequencing suggested a greater number of tumor-like cells, fibroblasts and mono-nuclear macrophages within the tumor microenvironment. The above results indicated that TSC-RAML exhibited a characteristic and disease-associated plasma proteomic profile. The unique microenvironment, made up of fibroblasts and mono-macrophages, may promote tumorigenesis and TSC-RAML progression.

Correspondence to: Dr Lulu Jia, Clinical Research Center, National Center for Children's Health, Beijing Children's Hospital, Capital Medical University, 56 Nanlishilu Road, Xicheng, Beijing 100045, P.R. China
E-mail: jluyu@126.com

Dr Yushi Zhang, Department of Urology, Peking Union Medical College Hospital, Chinese Academy of Medical Science and Peking Union Medical College, 1 Shuaifuyuan Wangfujing, Dongcheng, Beijing 100730, P.R. China
E-mail: beijingzhangyushi@126.com

*Contributed equally

Abbreviations: AML, angiomyolipoma; DEGs, differentially expressed genes; DEPs, differentially expressed proteins; GO, Gene Ontology; GSEA, gene set enrichment analysis; LAM, lymphangiomyomatosis; MCP-1, monocyte chemoattractant protein-1; NATs, non-tumor normal tissues; PMEL, premelanosome protein; S-AML, sporadic angiomyolipoma; SEGA, subependymal giant cell astrocytoma; TSC, tuberous sclerosis complex; TSC-RAML, TSC-related AML; UPLC-MS, ultra-performance liquid chromatography-mass spectrometry; WBDB, whole-body disease burden; WGCNA, weighted gene correlation network analysis

Key words: tuberous sclerosis complex, proteomics, diagnostic markers, tumor microenvironment, UPLC-MS, RNA transcriptome

Introduction

Tuberous sclerosis complex (TSC) is a rare autosomal dominant disease, caused by the heterozygous germline mutations in TSC1 or TSC2 genes on chromosome 9 and 16, respectively. According to the research, the overall mutation detection rate among patients with TSC is 85-90% and 10-15% of patients were not identified (1). Regarding the pathologic mechanism for non-mutation patients with TSC, numerous theories have been put forward, including somatic mosaicism or intronic splicing variants affecting TSC1 or TSC2 (2). TSC affects multiple organs throughout the body, although two-thirds of all cases

are sporadic (1). According to research, the incidence within newborn children is 1:6,000-10,000. Without disentangling differences between ethnic groups or gender preferences (3), there are currently two million individuals living with TSC worldwide (2). Treatments for TSC require interdisciplinary cooperation and coordination from specialists within various fields, as TSC is characterized by hamartomas within multiple organs, including the brain, lungs, skin, kidneys, heart and eyes (3).

Angiomyolipomas are the most common type of TSC-related renal lesions, affecting 55-75% of all cases of TSC. The abnormal vasculature (including aneurysms) may result in spontaneous life-threatening bleeding, which is a leading cause of early death in adult patients with TSC (4-6). The pathological loss of heterozygosity resulting from tumor-suppressor mutation of TSC genes disables the inhibitory role in controlling mammalian target of rapamycin (mTOR). The mTOR pathway is a crucial signaling pathway in regulating cellular growth and metabolization, and overactive mTOR therefore leads to the formation of hamartoma (3,7). Accordingly, mTOR inhibitors such as everolimus have been approved for the treatment of TSC-associated renal angiomyolipoma (TSC-RAML) and subependymal giant cell astrocytoma (SEGA) (7). The Exist-2 study (NCT00790400) is a double-blind, placebo-controlled, phase III trial which confirmed the efficacy of everolimus in reducing renal angiomyolipoma volume with an acceptable safety profile (8). In addition, the Exist-2 trial indicated that the plasma levels of VEGF-D diminished after everolimus treatment, which correlated with the TSC-RAML volume, indicating that VEGF-D may be used as a prognostic marker (8).

Unlike sporadic angiomyolipoma (S-AML), TSC-RAML has unique pathologic behaviors, including bilateral, early onset in multiple sites (9). Therefore, questions remain regarding how to differentiate TSC-RAML from S-AML as a diagnostic marker, as well as the functional mechanism. Undoubtedly, its low prevalence limits the availability of the precious samples and feasibility of gaining insight into the mechanisms involved. The aim of the present study was therefore to identify potentially useful diagnostic markers and to assess their relationship with the tumor and whole-body burden, as well as to explore the tumor microenvironment.

Patients and methods

Patients and samples. A total of 25 consecutive patients with TSC diagnosed according to the 2012 diagnostic criteria from the International Tuberous Sclerosis Complex Consensus Conference (10) at Peking Union Medical College Hospital (Beijing, China) between November 2016 and November 2017 were enrolled. All participants were ≥18 years old and had at least 1 TSC-RAML with a size of >3 cm. All participants were subjected to next-generation sequencing to identify TSC1 or TSC2 mutation types. Blood samples from patients with TSC at baseline and after 3-6 months of being administered everolimus were collected. Those without plasma samples in our sample bank or concurrent malignant tumors or metabolomic diseases, such as diabetes or hyperlipidemia, were excluded.

Maximum renal tumor volumes and pulmonary lymphangioleiomyomatosis (LAM) status were assessed independently by radiologists and respiratory physicians using computed tomography in a clinical setting. In addition, another 25 patients with renal cyst and 25 patients with S-AML were simultaneously enrolled to establish a control group. To further explore the tissue proteomics and transcriptome, 15 paired TSC-RAML tumor and non-tumor normal tissues (NATs) were collected from the surgery room of Peking Union Medical College Hospital (Beijing, China) between November 2016 and November 2021. After sample selection and quality control, 8 paired TSC-RAML tumor and NATs were enrolled into the following proteomic experiments, as well as 10 tumor and 8 NATs into the RNA sequencing experiments. In addition, proteomic experiments were also conducted on another cohort of 8 paired S-AML tumor and NATs during the same time period to establish control groups.

The present study was approved by the Institutional Review Board in Peking Union Medical College Hospital and the Institute of Basic Medical Sciences, Chinese Academy of Medical Sciences (Beijing, China; approval no. KS2020127). Informed consent was requested and obtained from each patient prior to being accepted to participate.

Genotype and phenotype. TSC gene mutations were further divided into five types, namely frameshift mutation, missense mutation, nonsense mutation, other mutations e.g. splicing abnormality and gene deletion, and no mutation. TSC-RAML was graded according to the Renal Angiomyolipoma Staging Criteria Proposed by the University Medical Center Utrecht: Stage 1 to 6 (11). The LAM status was determined by radiologists and respiratory specialists in this field and graded as either 0 (without LAM) or 1 (with LAM). The whole-body disease burden was calculated for each participant as the sum of AML grading and LAM status, with scores ranging from 1 to 7.

Plasma and tissue proteomics according to ultra-performance liquid chromatography mass spectrometry (UPLC-MS)

Plasma sample collection and pre-experiment processing. For blood samples, 4 ml EDTA tubes, containing whole blood, were collected in the morning between 07:00-09:00 am after overnight fasting to reduce the effect of the diet. Plasma and peripheral blood mononuclear cells were isolated through density gradient centrifugation over Ficoll-Hypaque, at room temperature, within 1 h of initial collection. The plasma layer was extracted and then stored at -80˚C until the formal experiment.

High Select™ Top14 Abundant Protein Depletion Mini Spin Columns (Thermo Fisher Scientific, Inc.) were applied to eliminate extraneous proteins in the plasma following the manufacturer's instructions and 30-μl samples were obtained after the above process. From each sample, 10 μl were removed to measure protein concentrations using the Pierce™ BCA assay protein assay kit (cat. no. 23225; Thermo Fisher Scientific, Inc.).

Tissue sample preparation for proteomics. Tumor tissues and NATs were removed in the operation room and were transferred into liquid nitrogen within 0.5 h and preserved until the experiments took place. Approximately 25-120 mg tissue was homogenized separately in an appropriate volume of lysis buffer [i.e. 2% SDS, 20 mM Tris, cocktail (1:100 dilution),

DNAse (1:100 dilution), RNAse (1:1,000 dilution)] by repeated vortexing. The protein concentration was determined using the Pierce™ BCA assay protein assay kit.

Protein digestion. Dithiothreitol (20 mM for every 100 mg of protein within each sample) was applied for protein reduction for 5 min at 95˚C and subsequently alkylated with 50 mM iodoacetamide for 45 min at room temperature in the dark. The filter-aided sample preparation technique was performed to digest proteins and 30 kDa filter devices (Pall Filtersystems GmbH) were used. Trypsin (Trypsin Gold; mass spec grade; Promega Corporation) was added (enzyme to protein ratio, 1:50) and incubated at 37˚C overnight. After centrifugation at 14,000 x g (4˚C, 10 min), ~30 μl liquid was retrieved from each sample.

Quality control samples were taken from randomly selected representative samples and injected with formal samples. All of the samples were loaded on the autosamplers with a mixture of indexed retention time (iRT).

Electron spray ionization (ESI)-LC-MS/MS for proteome library generation. Pooled peptide samples of each group were separated by high-pH reverse phase LC columns (4.6x250 mm, C18, 3 μm; Waters Corporation) and then loaded onto the column in buffer A1 (H_2O; pH 10) using a Waters H-class UPLC (Waters Corporation). The elution gradient was 5-30% buffer B1 [90% acetonitrile (ACN); pH 10; flow rate, 1 ml/min] over 30 min.

The eluted peptides were collected at one fraction per minute. After lyophilization using a CENTRIVAP (ChristRVC 2-25 CD plus; Martin Christ GmbH), the 30 fractions were resuspended in 0.1% formic acid and then concatenated into 10 fractions by combining fractions 1, 11, 21, etc. To generate the spectral library, the fractions from RPLC were analyzed in data-dependent acquisition (DDA) mode using an EXPLORIS 480 (Thermo Fisher Scientific, Inc.). The parameters were set as follows: the MS was recorded at 350-1,500 m/z at a resolution of 60,000 m/z; the maximum injection time was 50 msec, the auto gain control (AGC) was $1x10^6$, and the cycle time was 3 sec. MS/MS scans were performed at a resolution of 15,000 with an isolation window of 1.6 Da and high-collision dissociation (HCD) collision energy of 32%; the AGC target was 50,000 and the maximum injection time was 30 msec.

ESI-LC-MS/MS for proteome data-independent acquisition analysis. Digested peptides were dissolved in 0.1% formic acid and separated on an RP C18 self-packing capillary LC column (75 μm x 150 mm, 3 μm; Dr Masch GmbH). The eluted gradient was 5-30% buffer B2 (0.1% formic acid and 99.9% ACN; flow rate, 0.3 μl/min) for 60 min. For MS acquisition, the variable isolation window data-independent acquisition (DIA) method with 38 windows was developed. The specific window lists were constructed based on the DDA experiment of the pooled sample. The full scan was set at a resolution of 120,000 over the m/z range of 400 to 900, followed by DIA scans with a resolution of 30,000; the HCD collision energy was 32%, the AGC target was 1E6 and the maximal injection time was 50 msec.

Spectral library generation. To generate a comprehensive spectral library, a pooled sample from each group was processed. DDA data were processed using Proteome Discoverer software (Thermo Fisher Scientific, Inc.) and searched against the human UniProt database (https://sparql.uniprot.org/) appended with the iRT fusion protein sequence (Biognosys AG).

A maximum of two missed cleavages for trypsin were used, cysteine carbamidomethylation was set as a fixed modification and methionine oxidation deamination and +43 on Kn (Carbamyl) were used as variable modifications. Parent and fragment ion mass tolerances were set to 10 ppm and 0.02 Da, respectively. The applied false discovery rate (FDR) cut-off was 0.01 at the protein level. The results were then imported to Spectronaut Pulsar software (Biognosys AG) to generate the spectral library.

In addition, DIA data were imported into Spectronaut Pulsar software and searched against the human UniProt database to generate the DIA library. The final library was generated by combining the DDA and DIA libraries of all samples.

Data analysis. DIA-MS data were analyzed using Spectronaut Pulsar (Biognosys AG) with default settings. All results were filtered with a Q-value cutoff of 0.01 which corresponded to an FDR of 1%. Proteins identified in >50% of the samples in each group were retained for further analysis. Missing values were imputed based on the k-nearest neighbor method.

Raw proteomics data were transformed with log2 and then centralized. Supervised orthogonal partial least squares discriminant analysis (O2PLS-DA) was applied to view the distribution tendency of all samples with SIMCA version 14.1 (Umetrics). The unpaired, two-sided t-test was implemented to calculate the differentially expressed proteins with the software R v4.1.1 (https://www.r-project.org/).

Bulk RNA sequencing

RNA quantification and qualification. A total of 10 TSC-RAML tumor tissues and 8 paired non-tumor normal tissues samples were resected from the operation room and stored at -80˚C until final analysis. Subsequently, total RNA was isolated from the above tissue using TRIzol (Invitrogen; Thermo Fisher Scientific, Inc.). RNA integrity was assessed using the RNA Nano 6000 Assay Kit from the Bioanalyzer 2100 system (Agilent Technologies, Inc.). The following RNA-seq experiments were performed by Novogene (Beijing, China).

Library preparation for transcriptome sequencing. NEBNext® Ultra™ RNA Library Prep Kit for Illumina® (New England Biolabs, Inc.) was used to construct sequencing libraries following the manufacturer's recommendations. Total RNA was used as input material for RNA sample preparations. mRNA was purified using poly-T oligo-attached magnetic beads. Fragmentation was performed using divalent cations at an elevated temperature in First Strand Synthesis Reaction Buffer (5X). First strand cDNA was synthesized using random hexamer primer and M-MuLV Reverse Transcriptase, then RNaseH was used to degrade the RNA. Second strand cDNA synthesis was subsequently performed using DNA Polymerase I and dNTP. Remanent overhangs were converted into blunt ends through exonuclease/polymerase activities. After adenylation of 3' ends of DNA fragments, adaptors with hairpin loop structures were ligated to prepare for hybridization. In order to select cDNA fragments of preferentially 370-420 bp in length, the library fragments were purified with an AMPure

XP system (Beckman Coulter, Inc.). Subsequently, PCR was performed using Phusion High-Fidelity DNA polymerase, Universal PCR primers and an Index (X) Primer according to a previously published protocol (12). PCR products were purified (AMPure XP system; Beckman Coulter, Inc.) and the library quality was assessed on the Agilent Bioanalyzer 2100 system (Agilent Technologies, Inc.).

Clustering and sequencing. This experiment was performed at the Novogene Experimental Department. The clustering of the index-coded samples was performed on a cBot Cluster Generation System using TruSeq PE Cluster Kit v3-cBot-HS (Illumia, Inc.) according to the manufacturer's instructions. After cluster generation, the library preparations were sequenced on an Illumina Novaseq platform and 150 bp paired-end reads were generated.

Data processing and differential analysis. Raw data (raw reads) in the fastq format were first processed through in-house perl scripts. Reads mapping to the reference genome (GRCh38) and gene model annotation files were downloaded from the genome website directly (http://www.ensembl.org/Homo_sapiens/Info/Index). Paired-end clean reads were aligned to the reference genome using Hisat2 v2.0.5 (http://daehwankimlab.github.io/hisat2/). For the quantification of gene expression levels, featureCounts v1.5.0-p3 (http://subread.sourceforge.net/) was used to count the number of reads mapped to each gene. Subsequently, the FPKM of each gene was calculated based on the length of the gene and the reads count was mapped to this gene.

Differential expression analysis was performed using the DESeq2 R package v1.20.0. The resulting P-values were adjusted using the Benjamini-Hochberg approach for controlling the FDR. Genes with an adjusted P<0.05 were assigned as being differentially expressed.

Single-cell RNA sequencing. The single-cell RNA sequencing data (10X data) of a patient with TSC1-mutated AML were downloaded from the Gene Expression Omnibus (GEO) database (https://www.ncbi.nlm.nih.gov/geo/; GEO accession no. GSM4035469) and used to simulate the microenvironment of TSC-RAML, which has been analyzed and presented in the original study by Guo *et al* (13). In addition, the raw experimental procedures are available in the original article and the following steps describe the quality control and analytic process.

The quality control and secondary analysis were conducted with R v4.1.1 and the Seurate package (14,15). Cells with a mitochondrial gene percentage of >30% and with <200 genes and >2,500 genes were filtered. After this selection, 1,675 high-quality cells were obtained for further analysis. After normalization scaling of the raw data, all highly variable genes were included into the downstream primary component analysis. Elbow-plot analysis was used to identify significant principal components. With the resolution of 0.5, all the cells were classified into 10 groups. The differentially expressed genes (DEGs) within groups were found with the FindAllMarkers function and the cells were firstly annotated by the R package 'SingleR' (16) automatically and then annotated manually through searching published articles. The top 200 ranked genes from each cell were then selected to perform gene ontology analysis with the R package 'clusterProfiler' (17,18). The R package 'monocle' (version 2.24.1) was used to construct the pseudo-time trajectories (19).

Functional analysis. The Gene Ontology (GO) functional enrichment was performed with the R package 'clusterProfiler' (17,18). The characteristic modules of each subgroup were completed by the weighted gene correlation network analysis '(WGCNA)' package (20,21) and the correlation between modules and clinical information was assessed by Pearson correlation analysis. The Gene Set Enrichment Analysis (GSEA) application (version 4.1.0) was applied to perform GSEA hallmark analysis. The cell composition within the tumor microenvironment was calculated with the R package 'MCPcounter' (22).

Statistical analysis. Unless specially mentioned above, all the data analyses were performed and figures were generated using R (version 4.1.1) with required packages described in the sections above. χ^2 and Kruskal-Wallis tests were used to assess the gender and age distribution within different subgroups. All of the tests were two-sided and P≤0.05 was used as the threshold for statistical significance.

Results

Baseline information of enrolled patients. A total of 75 participants with 100 plasma samples were divided into four subgroups, namely the pre-treatment TSC-RAML (n=25), post-treatment TSC-RAML (n=25), S-AML (n=25) and renal cyst (CY, n=25) groups. The demographics and clinical information of the patients are summarized in Table I. Among the 25 patients with TSC-RAML, 36% (n=9) were male and the rates for S-AML and CY (renal cyst) were 20% (n=5) and 44% (n=11), respectively (P=0.186). In terms of age, the subjects in the TSC-RAML group were younger with a median age of 30 years old, compared with 39 for S-AML and 45 for CY (P<0.001).

In the genotype group (n=25), 76% (n=19) were indicated to have TSC2 gene mutations, and among these, nonsense mutations were the most frequent with 28% (n=7). This was followed by frameshift mutations in 20% (n=5), other mutations (16%; n=4) and then missense mutations (12%; n=3), as presented in Fig. S1A.

In the clinical phenotype group, most TSC-RAML grades were 5 and 6, and were therefore considered severe, suggesting a heavy renal tumor burden. Among the 25 participants, 10 had LAM (40%) and the median whole body disease burden was 5 (Table I).

Unique plasma proteomics of patients with TSC-RAML distinguished from cases of S-AML and renal cyst. After censoring and filling missing values, 903 proteins were selected for further analysis. First, O2PLS-DA analysis was performed with SIMCA (version 14.1) and a three-dimensional distribution of all the samples was established. TSC-RAML plasma proteomic profiling was distinguished from S-AML and renal cyst (Fig. S1B). From the heatmap, the characteristic plasma proteomics of TSC-RAML as well as the similarity within everolimus treatment were directly observed (Fig. 1).

Table I. Baseline information of all the enrolled patients.

Item	TSC-AML (n=25)	S-AML (n=25)	CY (n=25)
Sex			
Male	9	5	11
Female	16	20	14
Age, years	30 (18-42)	39 (15-54)	45 (13-57)
Gene mutation type			
TSC2	19	-	-
None	6	-	-
AML grading			
1	3	-	-
2	2	-	-
3	3	-	-
4	1	-	-
5	7	-	-
6	9	-	-
LAM			
Yes	10	-	-
No	15	-	-
Whole body disease burden[a]	5 (1-7)	-	-

Values are expressed as n or median (range). [a]Whole body disease burden was defined as the sum of AML grading and LAM score. AML, angiomyolipoma; S-AML, sporadic AML; TSC, tuberous sclerosis complex; CY, renal cyst; LAM, lymphangiomyomatosis.

Differential analysis was applied to search for TSC-RAML-specific plasma proteins, regardless of the everolimus treatment status. In the volcano plots in Fig. 2A, it is apparent that numerous proteins, such as the upregulated MMP9, C-C motif chemokine ligand 5 (CCL5), premelanosome protein (PMEL) and the downregulated FGB, FGG, EPB41, appear to have differential roles, not only in TSC-RAML as opposed to renal cysts, but also in TSC-RAML vs. S-AML. PMEL (also known as HMB45) has already been regarded as a diagnostic marker for angiomyolipoma and MMP9 has been indicated to be elevated in TSC-related cortical tubes and subependymal giant cell astrocytoma at both the protein and transcriptome level (23,24). The Venn diagram revealed that there existed 71 proteins demonstrating similar differential functions like PMEL and CCL5 (Fig. 2A, lower panel).

Proinflammatory chemokine CCL5, responsible for recruiting immune cells such as monocytes and T cells to the site of inflammation (25), is significantly upregulated in TSC-RAML, suggesting a high inflammatory status. The functional enrichment analysis of differentially expressed proteins (DEPs) indicated that they were mostly enriched in the platelet degranulation, blood coagulation, hemostasis (category biological process), secretory granule lumen, cytoplasmic vesicle lumen, vesicle lumen (category cellular component) and actin binding, sulfur compound binding and glycosaminoglycan binding (category molecular function). The DEPs mainly participated in the process of blood cell function, secretory lumen component and actin binding function (Fig. 2B-D).

Relationship between plasma proteomics with LAM and gene mutation status. Previous research has reported that serum proteins such as VEGF-D may be prognostic markers not only for TSC-RAML (8), but also for TSC-LAM (26). Therefore, the impact of LAM on plasma proteomics was explored in the present study. The volcano plots and heatmaps in Fig. 3A and B suggest that the existence of LAM does not appear to influence the plasma proteomics because among the 903 proteins, only 16 pretreatment and 17 post-treatment molecules were statistically significant. It has been proposed that TSC2 gene mutation and those producing premature termination codons may lead to a severe phenotype (27,28). For plasma proteomics, it appears that a TSC2 mutation prior to treatment has a substantial influence on patients with 31 DEPs and S100 family members, such as S100A6, -A9 and -A12, had a tendency to be upregulated among patients with TSC2 mutation, which has been proved to engage in the neutrophil and macrophage accumulation, corresponding cytokine secretion and smooth muscle cell proliferation (29-32). However, after receiving everolimus, the number of DEPs was markedly reduced (Fig. 3C and D), indicating a reversible pattern after treatment.

WGCNA analysis highlights relationship between plasma proteomics and disease burden. To assess the tumor burden-associated plasma markers, all the proteins were divided into seven whole proteome co-expression clusters using the WGCNA package (Fig. 4). The eigengene module (ME) MEturquoise was negatively associated with the AML grading and whole-body disease burden (WBDB), while MEred was positively associated with LAM. Functional enrichment of MEturquoise suggested that AML and the WBDB characteristic module were mostly enriched in hydrogen peroxide metabolic process, carbohydrate biosynthetic process and neutrophil-mediated immunity (Fig. 5A). However, the LAM-related module MEred was enriched in the pathway of complement activation, humoral immune response and B cell response (Fig. 5B). The analysis also indicated that age and gene mutation status were not directly associated with any module (Fig. 4B), suggesting the limited effect of age and gene mutation status on plasma proteomics.

Tissue proteomics of patients with TSC-RAML and WGCNA analysis. One of the problems in TSC-RAML mechanistic research is the scarcity of tissue samples, as it is not generally recommended to perform surgical interventions for TSC-RAML (33). To validate the above analytic results, nine tumor tissues and NATs from patients with TSC-RAML and S-AML were collected and proteomics analysis was performed with UPLC-MS. Compared with the plasma, protein diversity in the tumor microenvironment was much higher with 6,178 proteins detected (Fig. 6).

From the heatmap in Fig. 6, a relative similarity between TSC-RAML and S-AML tumors, as well as a similarity between TSC-AML and S-AML NATs, was also observed.

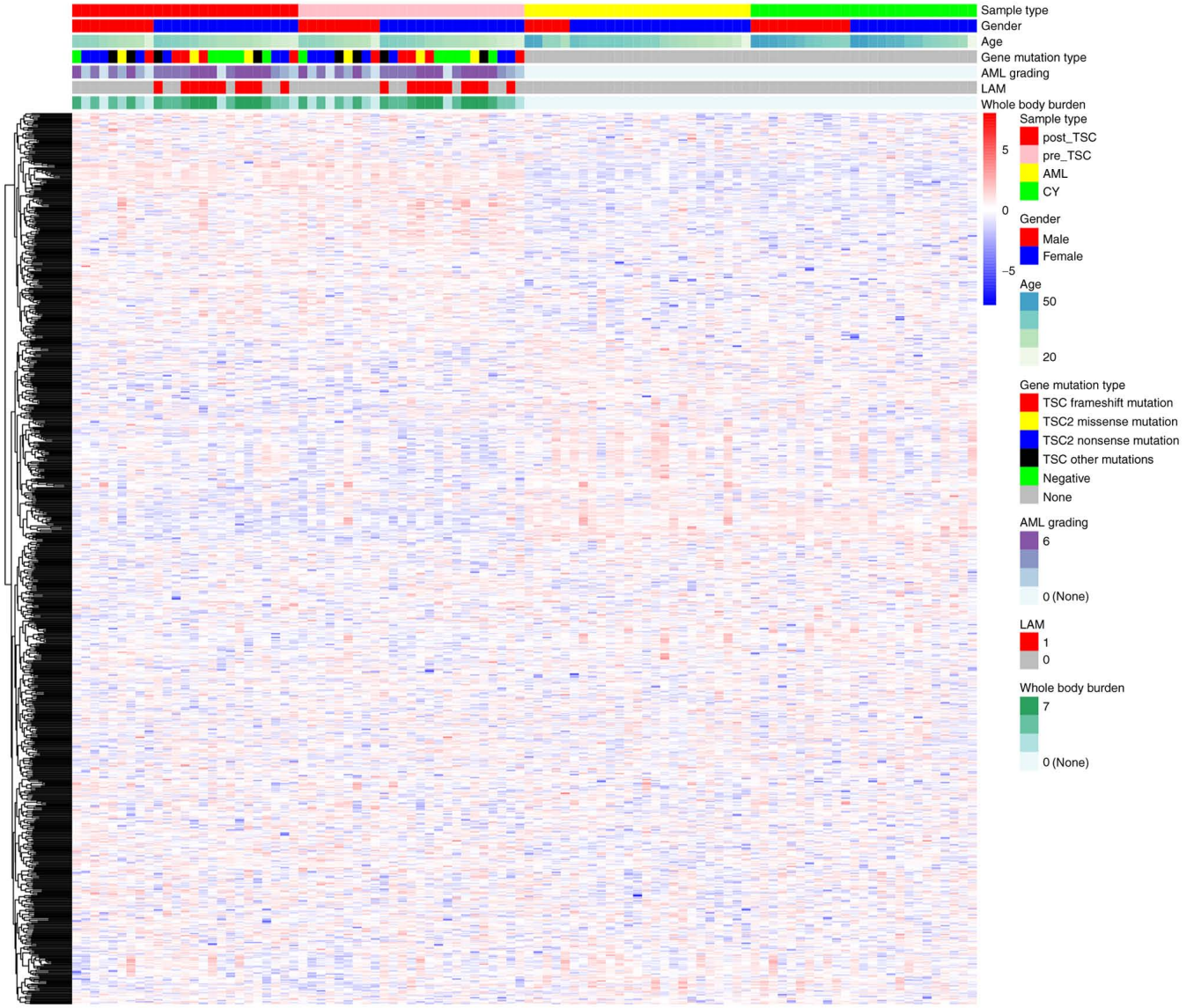

Figure 1. Relationship between plasma proteomics expression and clinical information. AML, angiomyolipoma; TSC, tuberous sclerosis complex; LAM, lymphangiomyomatosis.

However, the difference between tumors and NATs appeared distinct. Among the 6,178 total proteins, there existed 307 significantly upregulated and 616 downregulated proteins for TSC-RAML together with 417 upregulated and 687 downregulated proteins for S-AML (depicted in Fig. 7A, top and middle panels). GO enrichment of DEPs further validated the above result, as both TSC-RAML and S-AML had a similar enrichment result, namely altered small molecule catabolic process, mitochondrial matrix component and actin binding function. Both TSC-RAML and S-AML appeared to have altered lipid metabolization, including lipid catabolic process, cellular lipid catabolic metabolism and the fatty acid catabolic process (Fig. 7B, top and middle panels).

To explore TSC-RAML-specific protein patterns, intersected proteins with S-AML were deleted and the enrichment result indicated that ATP metabolic process, organic compound oxidation, oxidative phosphorylation, mitochondrial-associated compounds and actin binding were the most significantly distinguished pathways involved (Fig. 7A-D, lower panel). Additional WGCNA analysis revealed that MEbrown and MEturquoise were positively and negatively associated with TSC-RAML, respectively (Fig. 8A and B). Functional analysis of the two modules (Fig. 8C and D) highlighted the significant terms of small molecule catabolic process, organic acid catabolic process (MEbrown; all GO terms) and translational initiation and nuclear-transcribed mRNA catabolic process (MEturquoise; all GO terms), which have been reported previously by Lam *et al* (33).

Tissue RNA sequencing data reveal characteristic transcriptome of TSC-RAML and its unique tumor microenvironment composition. Altered proteomics may reflect upstream changes in RNA transcriptomes. Therefore, another cohort of TSC-RAML and NATs was also tested (raw data are provided in Table SI). From the heatmap, distinguished RNA profiling was clearly observed (Fig. 9A). GO enrichment indicated that the altered RNAs were mostly enriched in the pathways of divalent inorganic cation homeostasis, apical part

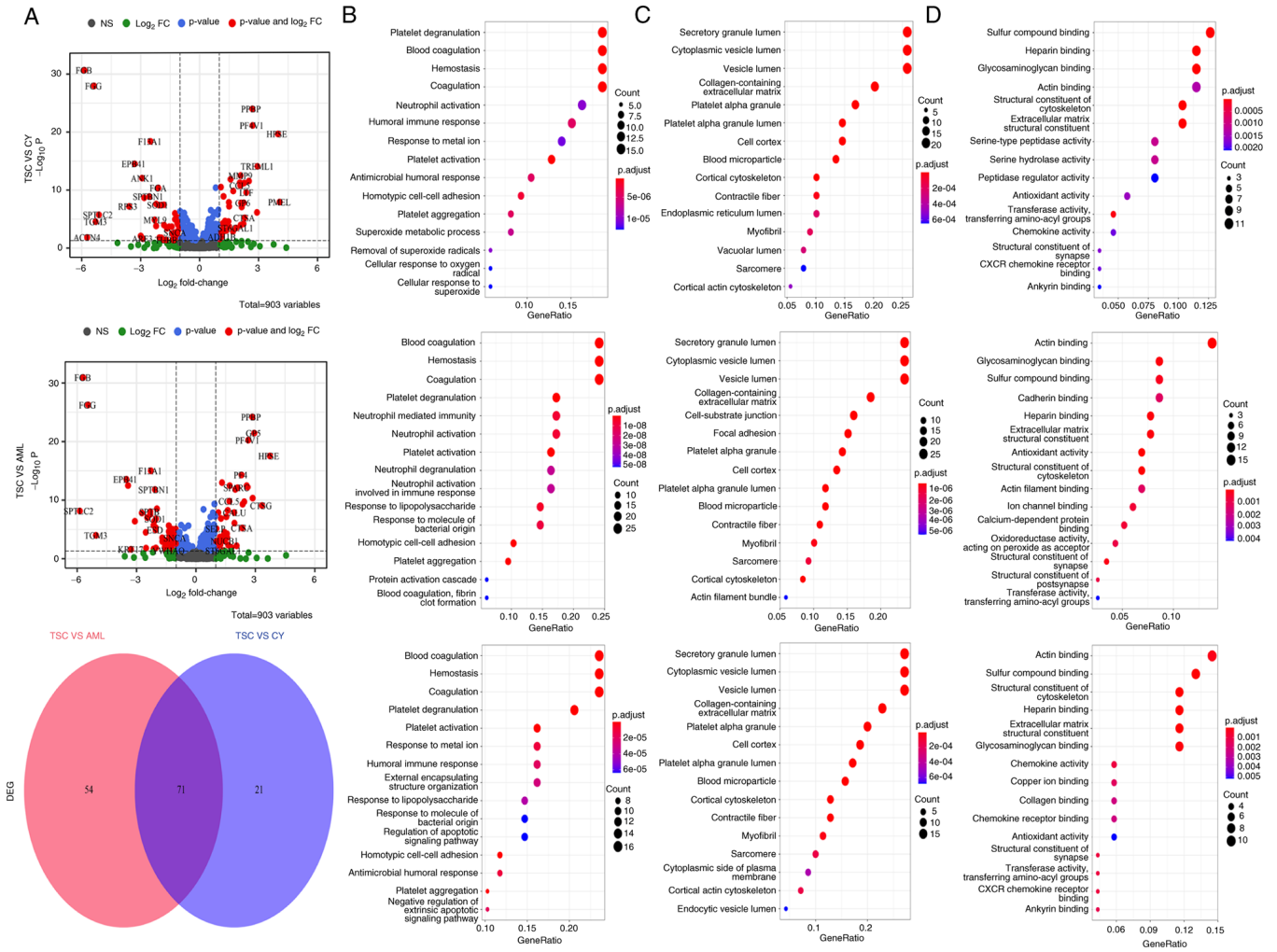

Figure 2. Plasma proteomics differential and functional enrichment analysis based on different subgroups. (A) The volcano (upper and middle panel) and Venn (lower panel) plots reveal differential and TSC-associated renal angiomyolipoma-specific proteins. (B) GO biological process enrichment of the differentially expressed proteins. (C) GO cellular component enrichment of the differentially expressed proteins. (D) GO molecular functional enrichment of the differentially expressed proteins. NS, no significance; FC, fold change; AML, angiomyolipoma; TSC, tuberous sclerosis complex; CY, renal cyst; DEG, differentially expressed gene; GO, Gene Ontology.

of cell, collagen-containing extracellular matrix and passive transmembrane transporter activity (Fig. 9B-D).

Compared with GO analysis, GSEA may better reveal the statistically significant, concordant differences between two biological states by ranking the molecules (34,35). From the results, it was clear that myogenesis process (Fig. 10A) was significantly upregulated, while K-ras and early-phase estrogen response were downregulated (Fig. 10B and C). Another important process in energy production, oxidation phosphorylation, even though not statistically significant, exhibited an upregulation tendency in TSC-RAML (Fig. 10D).

The R package 'MCFcounter' allows for the calculation of the absolute abundance of eight immune and two stromal cell populations within the tumor microenvironment from transcriptomic data (22). It was observed that the fibroblast subpopulation within the sample of patients with TSC-RAML was significantly higher than that in NATs. Furthermore, the endothelial cells and B lineage exhibited a dramatic reduction, indicating the local immune insufficiency in TSC-RAML (Fig. 11A-C). Due to the critical role of antigen-presenting cells in the adaptive immune response, dendritic cells had a decreasing tendency, although not reaching statistical significance (P=0.055; Fig. 11D). Other cell compositional changes without significance are presented in Fig. S2.

Single-cell RNA sequencing identifies TSC-RAML-like tumor cells and pseudo-time trajectories analysis reveals the developmental routine of tumor cells. The above analysis highlighted abnormal stromal and immune cell composition within the tumor microenvironment, although direct evidence is lacking. Based on the previously published article (13), a second-time analysis was performed. After quality control, 1,675 high-quality cells with 17,076 RNAs were selected and then classified into 10 subgroups. After sequentially automatic and manual annotation, the 10 subgroups were further divided into eight cell types (Fig. 12). A heatmap of characteristic markers for each cell type is presented in Fig. S3.

The source of TSC-RAML cells has not been identified until now (33), although TSC-LAM has been suggested to have a uterine source (13). According to clinical markers and previous research (13), cells with high expression of PMEL, CTSK, FIGF, ESR1, HOXA11 and SLC35F1 were defined as

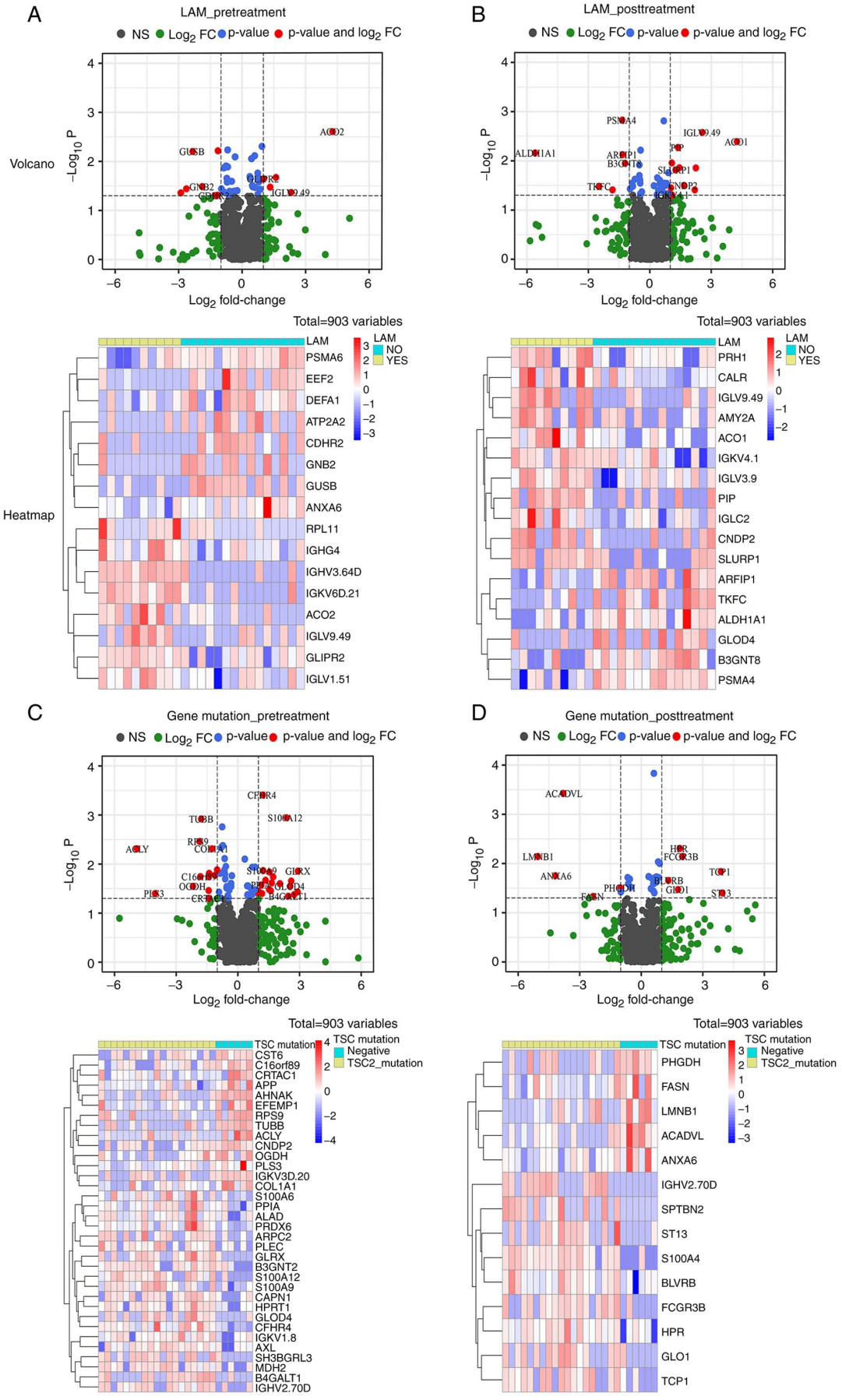

Figure 3. Impact of LAM and gene mutation status on plasma proteomics. (A) Pre-everolimus volcano plot reveals differential proteins and the corresponding heatmap based on the status of LAM. (B) Post-everolimus volcano plot reveals differential proteins and the corresponding heatmap based on the status of LAM. (C) Pre-everolimus volcano plot reveals differential proteins and the corresponding heatmap based on gene mutation. (D) Post-everolimus volcano plot reveals differential proteins and the corresponding heatmap based on gene mutation. LAM, lymphangiomyomatosis; NS, no significance; FC, fold change.

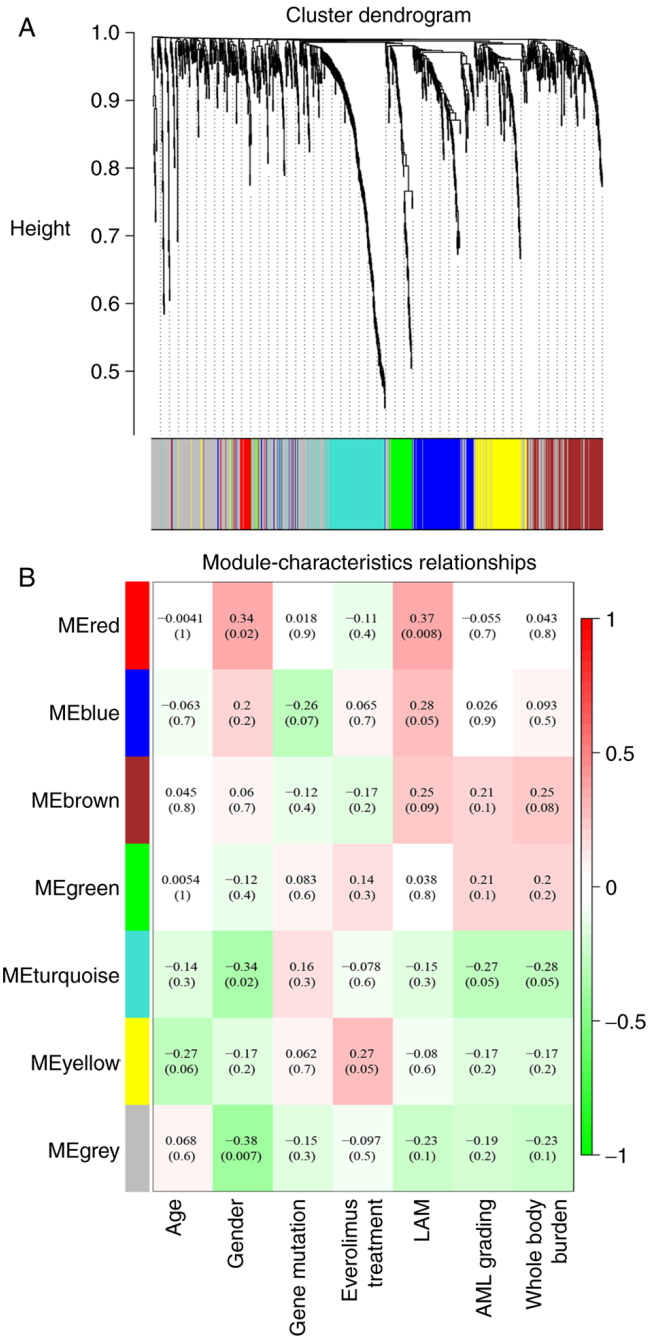

Figure 4. Weighted gene correlation network analysis identified seven modules and their correlation ship with local lesion and whole-body disease burden. (A) Dendrogram with clustering of differential co-expressed proteins (modules). (B) Correlation analysis identified local lesion (LAM: MEred; AML grading: MEturquoise)-related and whole-body disease burden (whole-body disease burden: MEturquoise)-related modules (correlation coefficients were located at the center of the modules with P-values in the brackets; method: Pearson correlation). LAM, lymphangiomyomatosis; AML, angiomyolipoma; ME, eigengene module.

tumor-like cells and the UMAP result is presented in Fig. S4. In terms of cell composition, accumulative monocytes and macrophages were observed together with a reduced number of T cells within the tumor microenvironment (percentage for monocytes, macrophages and T cells is 29, 15 and 7%, respectively). The functional enrichment of monocytes and macrophages suggested overactive neutrophil activation, increased secretory granules and increased actin binding process (depicted in Fig. S5). Another striking point is the similar RNA expression pattern of smooth muscle cells, fibroblasts and tumor-like cells (depicted in Fig. 12). The functional enrichment regarding the top 200 RNAs of tumor-like cells indicated that the differentially expressed genes (DEGs) are mainly involved in the muscle system process, ossification, collagen-containing extracellular matrix and actin binding (Fig. 13). Fibroblasts with $TSC^{-/-}$ have been widely applied in basic research to explore TSC mechanisms (36,37). From the GO analysis of fibroblasts, it was indicated that most of the DEGs were enriched in the process of ATP metabolic process, oxidative phosphorylation, mitochondrial composition and cadherin binding (Fig. S6).

Another way to explore the source and development of tumor cells is to simulate the differentiation lineage. Using the R package 'monocle' (19), developmental pseudo-time analyses of different cell types were drawn (Fig. 14), from which similar development between fibroblasts, smooth muscle and tumor-like cells was observed. This result is in accordance with the composition of TSC-RAML, namely vessels, smooth muscle and adipose (33).

Discussion

By retrospectively analyzing TSC-RAML, S-AML and renal cyst multi-omics data, the present study gained insight into the mechanisms of TSC-RAML, which may be summarized as follows: i) Plasma proteins such as MMP9 and CCL5 may be possible markers for TSC-RAML; ii) plasma proteomics enriched in neutrophil-mediated immunity, hydrogen peroxide and carbohydrate metabolic processes were associated with renal tumor grading and whole disease burden; and iii) tissue transcriptome revealed increased monocyte-macrophages within the tumor microenvironment, which may be crucial for TSC-RAML tumorigenesis and development.

In addition to TSC-RAML plasma proteomics analysis, the tissue transcriptome was also examined and indicated elevated MMP9. MMPs, containing a group of zinc-dependent endopeptidases, are responsible for remodeling the extracellular matrix collagen and elastin under pathological and physiological conditions (38). Previous studies (24,39) have also reported higher MMP9 mRNA and protein expression in TSC brain tubers compared to controls and peritubular brain tissues. In LAM, one of the most common pulmonary manifestations of TSC, MMP-9 has been detected at high levels in both serum and urine (40). This has been associated with loss of pulmonary function in LAM (38,40). Through Src kinase activation, MMP9 has been suggested to promote the invasiveness of TSC2-null embryonic fibroblasts *in vitro* (40,41). The inhibitor of MMP9 and MMP2, doxycycline, has demonstrated an anti-migration effect on TSC2-negative mouse embryonic fibroblasts (MEF) through downregulating RhoA-GTPase activity and phosphorylation of focal adhesion kinase (36). All evidence suggests that MMPs have a role in the tumorigenesis of TSC-related diseases. A recent study has also suggested that an axis containing CD147-MMP-VEGF increases tumor angiogenesis (40). This appears to be in accordance with the plasma elevated MMPs and VEGF-D related to TSC. In the present study, it was first observed that MMP9 was elevated not only in the blood of patients with

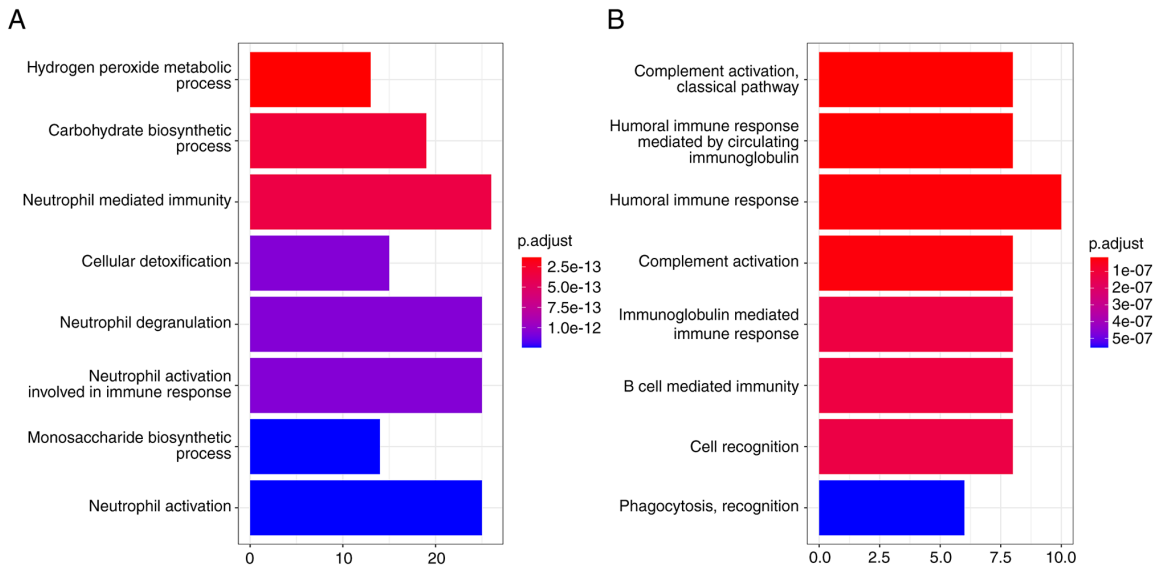

Figure 5. GO enrichment regarding proteins in the MEturquoise and MEred modules. (A) GO enrichment results of tuberous sclerosis complex-associated renal angiomyolipoma and whole-body disease burden associated module MEturquoise. (B) GO enrichment results of lymphangiomyomatosis-associated module MEred. GO, Gene Ontology; ME, eigengene module.

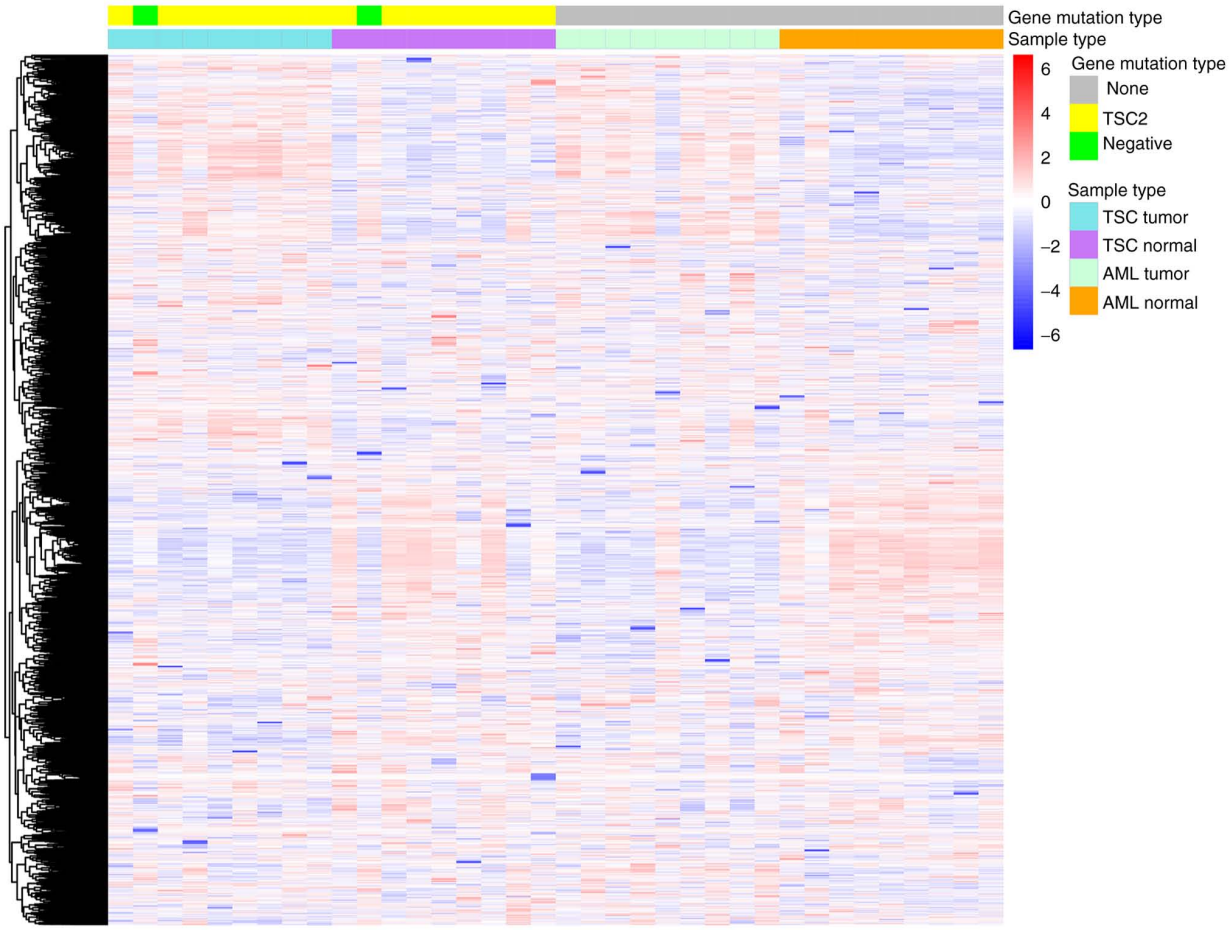

Figure 6. Relationship between tissue proteomics expression and basic clinical information. AML, angiomyolipoma; TSC, tuberous sclerosis complex.

TSC-RAML but also in the tissue transcriptome. Although further research is required to validate the present results, MMP9 may be suggested as a possible marker and drug target for TSC-RAML.

In addition to MMP9, CCL5, which is a member of the CC subfamily of chemokines, also appeared to have good distinguishability. CCL5 was able to be expressed on most inflammatory cell types, although monocytes and

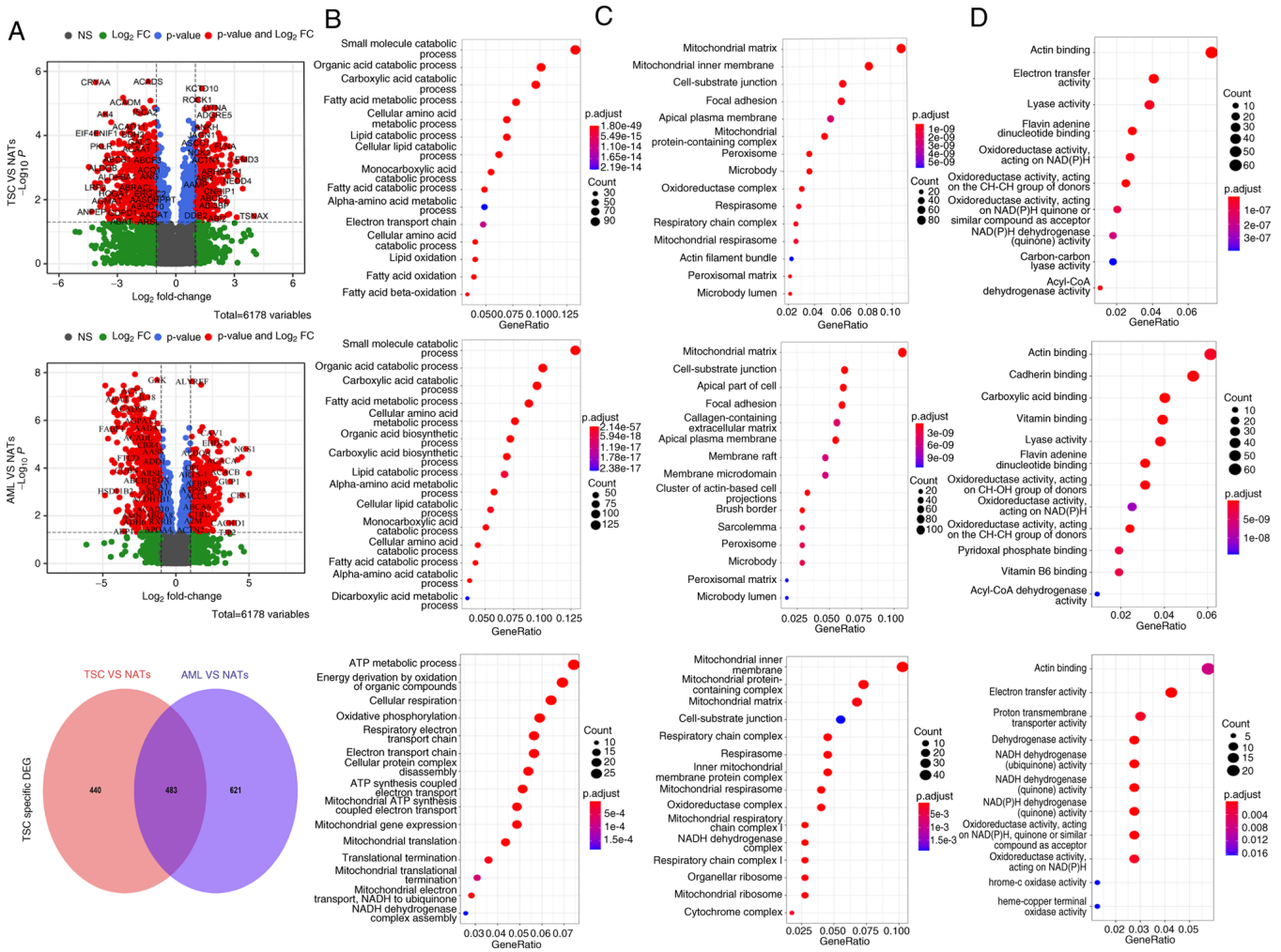

Figure 7. Tissue proteomics differential and functional analysis based on different subgroups. (A) The volcano (upper and middle panel) and Venn (lower panel) plots reveal differential and TSC-associated renal angiomyolipoma-specific proteins. (B) GO biological process enrichment. (C) GO cellular component enrichment. (D) GO molecular functional enrichment. NS, no significance; FC, fold change; AML, angiomyolipoma; TSC, tuberous sclerosis complex; DEG, differentially expressed gene; GO, Gene Ontology; NATs, non-tumor normal tissues.

T cells are the most common CCL5-expressing cells (25). Accumulating evidence suggests that CCL5 participates in numerous processes, including inflammation, cancers, viral infection and immune responses (25). Recent research has also indicated that plasminogen activator inhibitor-1 is able to regulate CCL5 and promote cell migration and angiogenesis and inhibit cell apoptosis through MMPs (25), suggesting there is a synergistic function between CCL5 and MMPs in tumorigenesis. William *et al* (42) reported that treatment of wild-type murine marrow-derived macrophages with mTORC1 inhibitors promoted 4E-BP1/2 activation and reduced CCL5 secretion, indicating that overactive mTOR and downstream 4E-BP1/2 may increase the production of CCL5. Accumulating evidence suggested that, as a chemoattractant factor, CCL5 was able to recruit tumor-associated macrophages (TAMs) to the tumor beds, thus facilitating tumor metastasis (43-45). In addition, TAMs have been proven to increase the secretion of collagen and thus potentiate the cell migration and increase tissue stiffness (43). Based on the results of the present study, plasma CCL5 was elevated and a large quantity of monocytes and macrophages was deposited within the tumor microenvironment according to single-cell RNA sequencing. Therefore, it may be proposed that high levels of CCL5 are necessary for modulating and recruiting monocyte-macrophages towards the tumor site and thus promoting tumor growth, although further experiments are required to confirm this finding.

Although a large number of studies have focused on genotype-phenotype correlation, no definite conclusion regarding TSC-RAML has been made, unless the TSC2 mutation is much more severe than that of TSC1 (27,28,46,47). A relatively large systematic review including 261 patients with TSC suggested that TSC1 missense mutation and the mutation of TSC2 encoding TAD1 were associated with a high risk of TSC-RAML (28). The present study attempted to find the proteins associated with phenotype. The results suggested that the proteins involved in metabolization, neutrophil-mediated immunity and extracellular matrix organization were significantly associated with renal tumor grading and whole-body disease burden. The present results were consistent with established plasma markers, namely elevated MMPs (reflecting the extracellular matrix organization) and CCL5, which participates in immune responses. In the aspect of metabolization, Bottolo *et al* (48) indicated that metabolites involving

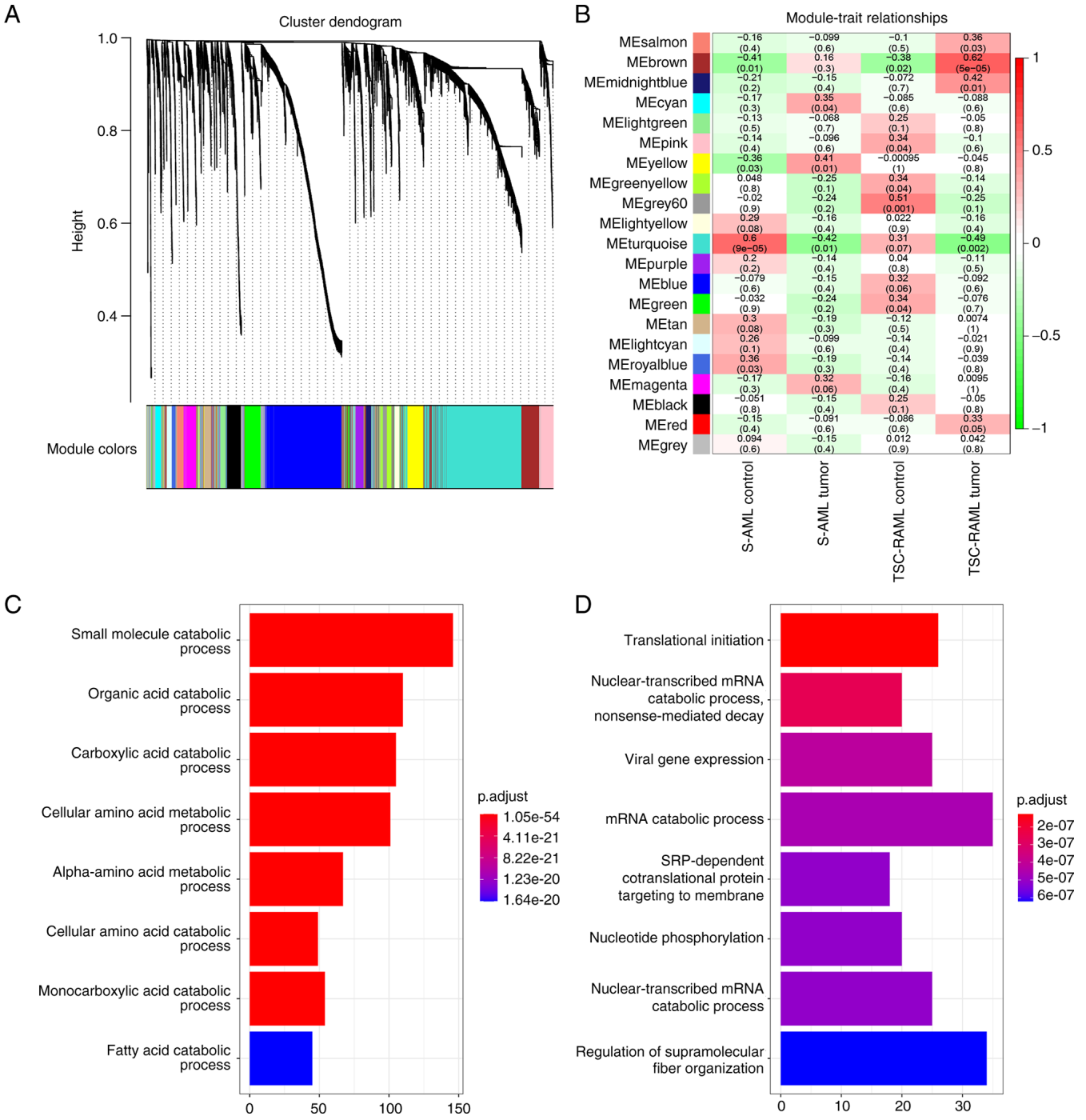

Figure 8. Tissue proteomics weighted gene correlation network analysis and functional analysis of TSC-RAML related modules. (A) Dendrogram providing clustering of differential co-expressed proteins (modules). (B) A total of 21 total modules and 5 significantly correlated modules were identified (correlation coefficients were located at the center of the modules with P-values in the brackets; method: Pearson correlation). (C) GO enrichment of the positively correlated module (MEbrown). (D) GO enrichment of the negatively correlated module (MEturquoise). TSC-RAML, tuberous sclerosis complex-associated renal angiomyolipoma; ME, eigengene module; S-AML, sporadic angiomyolipoma; GO, Gene Ontology.

fatty acid and sphingolipid metabolism were associated with the severity of lung disease, whole-body disease burden and disease activity. Feng *et al* (49) observed that secreted lysophospholipase D autotaxin (ATX) was upregulated in human renal angiomyolipoma-derived TSC2-deficient cells and inhibiting ATX was able to suppress TSC2 loss-associated oncogenicity *in vitro* and *in vivo* and induce apoptosis in TSC2-deficient cells. The tissue proteomic analysis of the present study indicated that both TSC-RAML and S-AML harbored a dysregulated lipid metabolism, further validating the notion that targeted lipid metabolism may be another breakthrough in treating TSC-related disease. From the RNA sequencing data, altered energy production was also observed, further validating the above analysis. It is generally thought that mTOR has a critical role in the regulation of metabolism and energy production (33). Although there was no difference in the components of TSC-RAML and S-AML, proteomics analysis revealed distinctive alterations of plasma and tissue

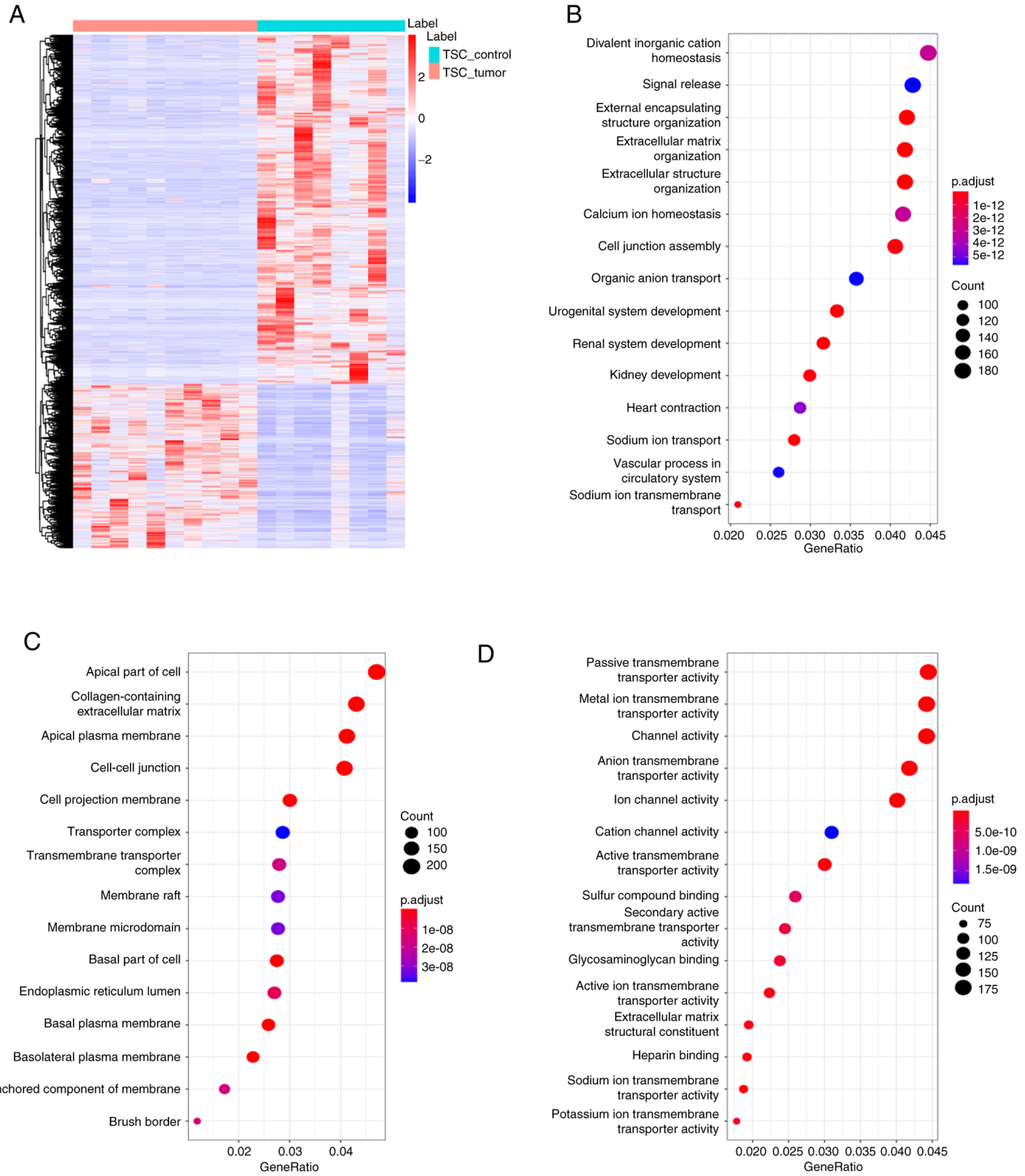

Figure 9. Differential and functional analysis of tissue transcriptome from patients with TSC-associated renal angiomyolipoma. (A) The differential analysis revealed that most genes were downregulated compared with para-tumor normal tissues. (B) GO biological process enrichment of DEGs. (C) GO cellular component enrichment of DEGs. (D) GO molecular functional enrichment of DEGs. GO, Gene Ontology; DEG, differentially expressed gene; TSC, tuberous sclerosis complex.

proteins. The RNA transcriptome analysis indicated that, compared with NATs, most of the differential RNAs were downregulated and the functional enrichment also revealed altered matrix organization and collagen-containing extracellular matrix.

Increasing evidence suggests that the cell composition within the tumor microenvironment has a critical role in tumorigenesis. From the RNA transcriptome data, the composition of 8 various cell types was determined in the present study. Fibroblasts were indicated to be higher in TSC-RAML

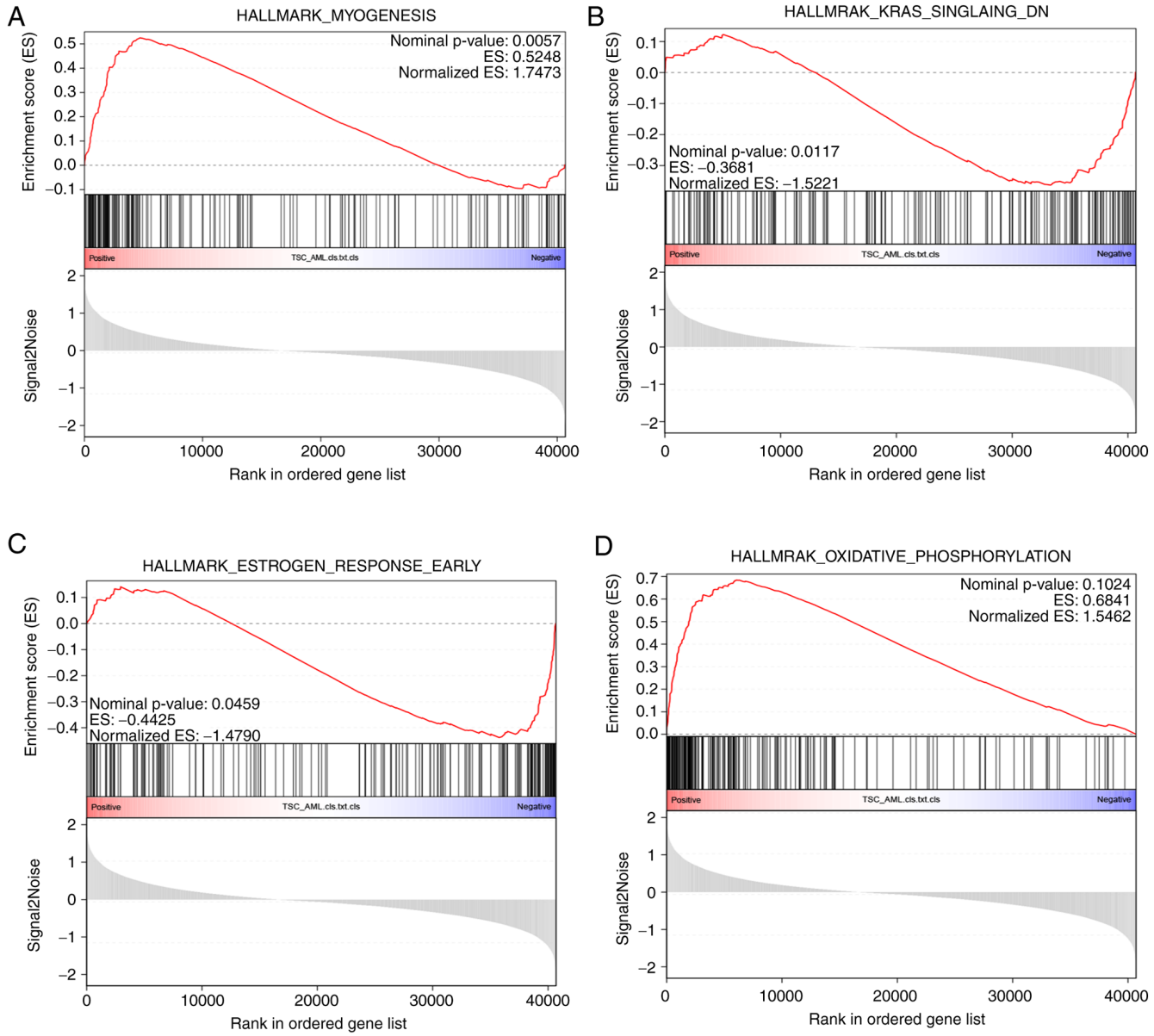

Figure 10. Top gene set enrichment analysis results for TSC-associated renal angiomyolipoma tissue transcriptome revealed (A) altered myogenesis, (B) k-ras signaling, (C) estrogen response and (D) oxidative phosphorylation. AML, angiomyolipoma; TSC, tuberous sclerosis complex; ES, enrichment score.

compared with NATs. A previous *in vitro* study suggested that TSC2-null fibroblast-like cells grown from human TSC skin hamartomas were able to induce normal human keratinocytes to form hair follicles and stimulate changes in hamartomata, suggesting that the fibroblast-like cells may be the source of the TSC tumor (50). In experiments using $TSC^{-/-}$ cell lines, MEFs with TSC2 knockout are still most widely used, indicating the similarity between fibroblasts and tumor cells in terms of biological behaviour (36,51). Another experiment discovered that a population of stromal cells/fibroblasts from the kidney labelled by Prx1 was able to form a cyst from the loop of Henle after ablation of the Tsc1 gene, indicating the contributive role of fibroblasts in patients with TSC (52). From the cell annotation for patients with TSC-RAML, the tumor-like cells were also identified, which had similarities with fibroblasts and smooth muscle cells. The pseudo-time analysis revealed a similar developing tendency of the three cell clusters, indicating their same source. All of the evidence suggested that the tumor cells, as well as fibroblasts and smooth muscle cells, may originate from the same progenitor cells.

Contrary to the increased fibroblasts, other cell types, including endothelial cells, B cells and DC cells, were decreased in TSC-RAML, suggesting an immune inhibitory state within the tumor microenvironment. In line with the RNA transcriptome, the single-cell RNA sequencing revealed a high proportion of monocytes and macrophages but low proportion of T cells. As reported, M2-like tumor-associated macrophages have critical roles in facilitating epithelial-mesenchymal transition, angiogenesis and immunosuppression (53). A previous *in vitro* experiment indicated that fibroblast-like cells from angiofibroma and periungual fibromas were able to secrete higher levels of monocyte chemoattractant protein-1 (MCP-1) mRNA and

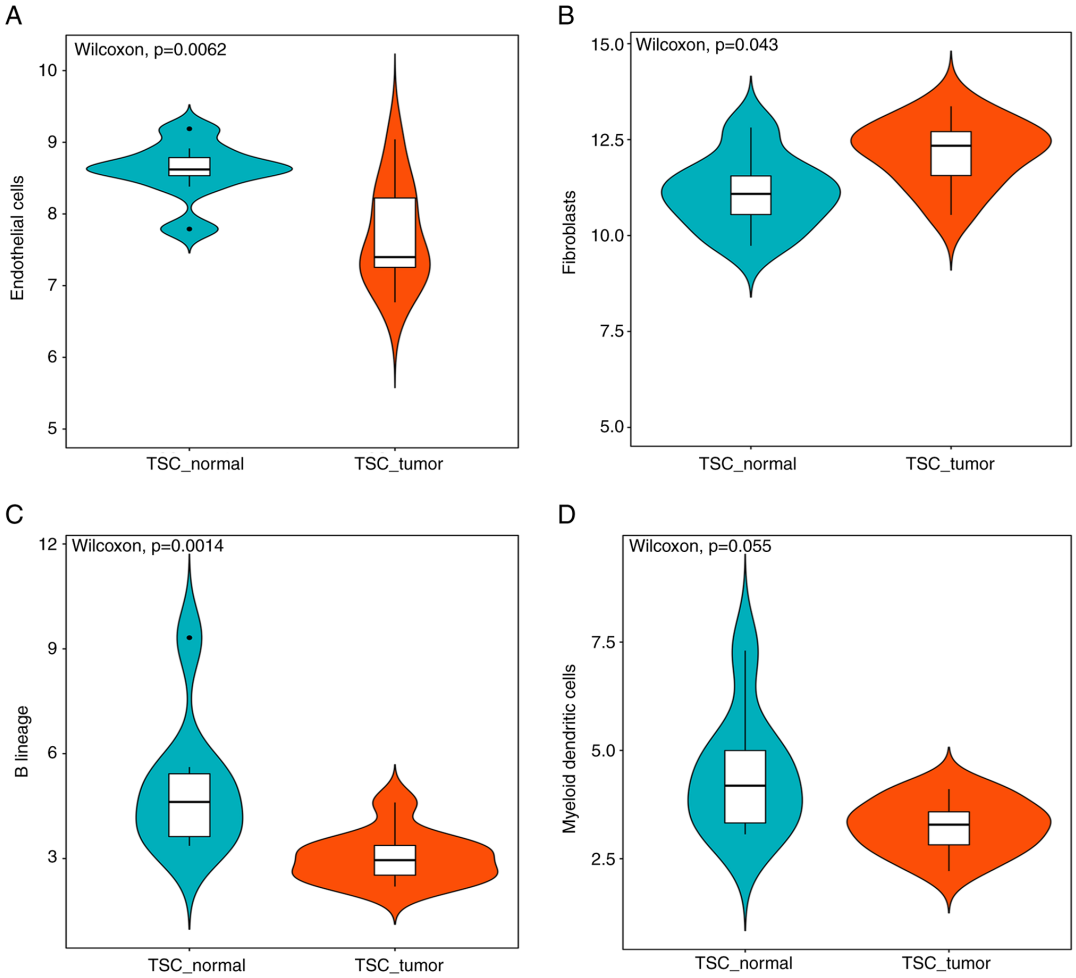

Figure 11. Stromal and immune cell compositions within the tumor microenvironment estimated using transcriptome analysis. (A) Endothelial cells were decreased, (B) fibroblasts were increased, and (C) B lineage cells and (D) myeloid dendritic cells were decreased within the TSC-associated renal angiomyolipoma tumor microenvironment compared with the para-tumor normal tissues. TSC, tuberous sclerosis complex.

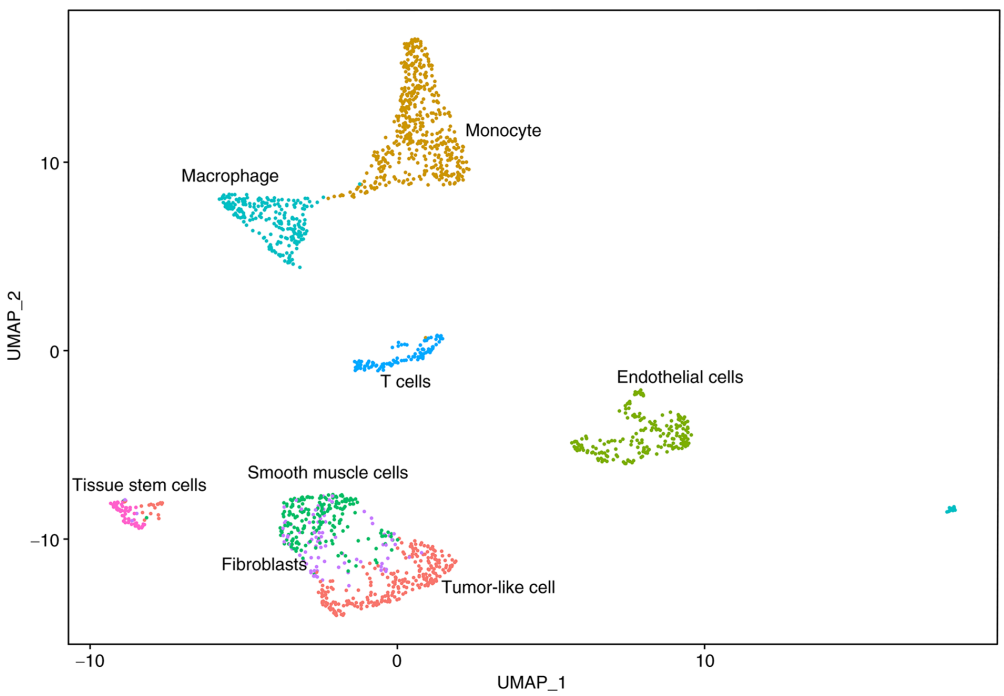

Figure 12. Clustering and annotation of single-cell RNA sequencing from one patient with TSC1 gene-mutated renal angiomyolipoma. UMAP, Uniform Manifold Approximation and Projection; TSC, tuberous sclerosis complex.

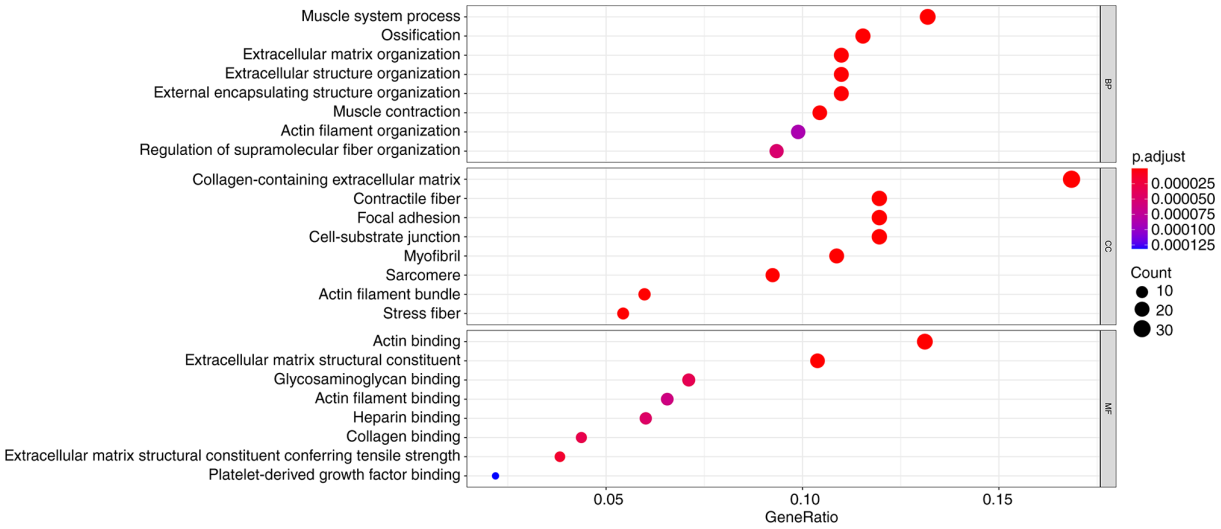

Figure 13. Gene ontology enrichment of TSC1 gene-mutated renal angiomyolipoma tumor-like cells. BP, biological process; CC, cellular component; MF, molecular function; TSC, tuberous sclerosis complex.

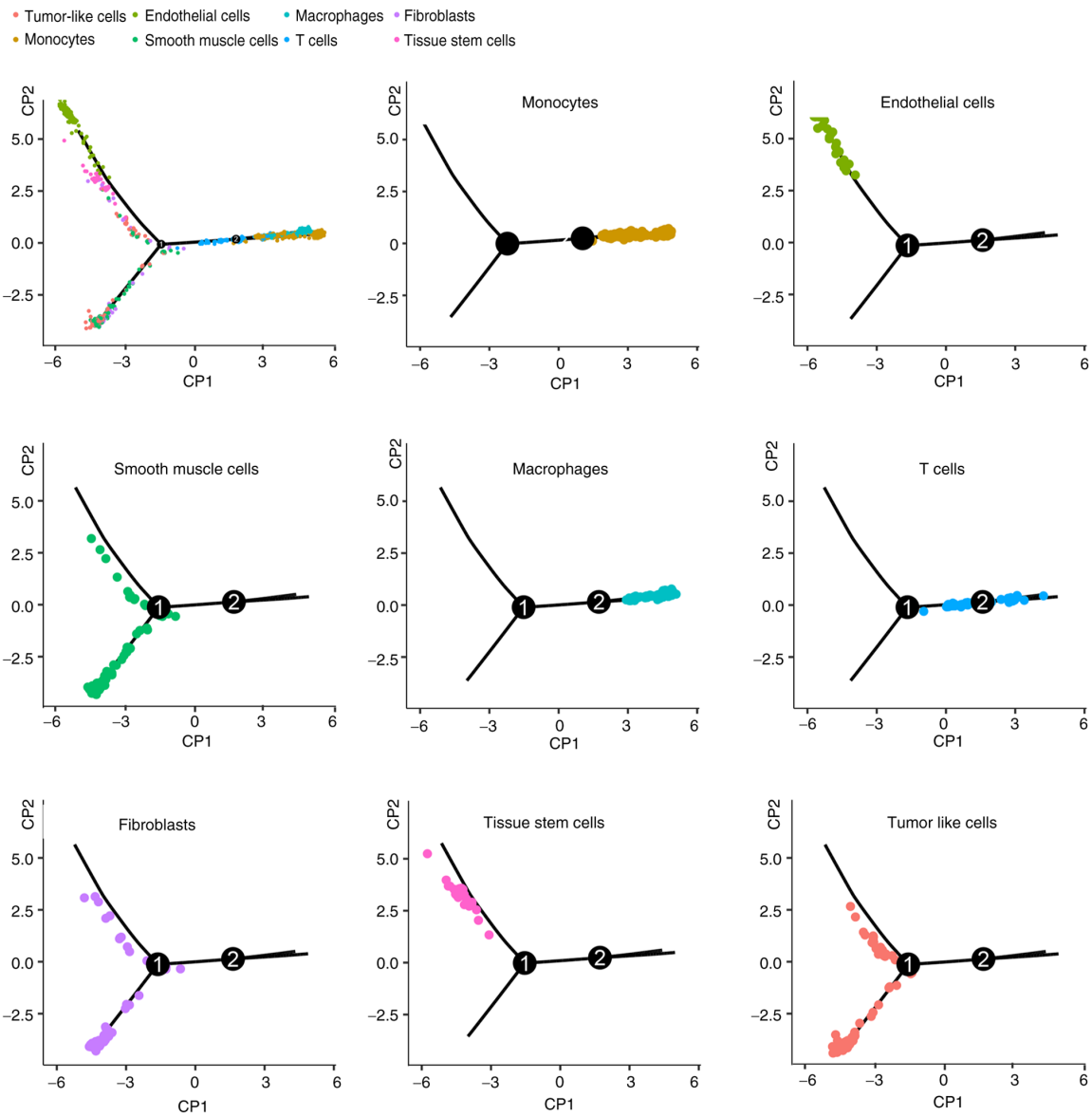

Figure 14. Pseudo-time trajectories analysis of all the cell types within the tumor microenvironment revealed similar developmental routines between fibroblasts, tumor-like and smooth muscle cells. CP, component.

protein than fibroblasts from the same patient's normal skin (54). Furthermore, conditioned medium from cultured TSC skin tumor cells was chemotactic for human monocytic cells and neutralizing antibody against MCP-1 inhibited the chemotactic activity (54). In line with this, Eker rat embryonic fibroblasts with TSC2 deletion produced 28 times higher MCP-1 protein compared with the wild-type (54). In a mouse model with TSC1 deletion, it was demonstrated that macrophages were refractory to IL-4-induced M2 polarization and evoked increased inflammatory responses to pro-inflammatory stimuli, suggesting the critical role of the mTOR pathway in regulating macrophage polarization (55). All of the above results validated the role of monocyte-macrophages in tumorigenesis and suggested a new therapeutic approach for TSC-related disease.

As exploratory research, the present study has the following limitations. First, the sample size in the present cohort was relatively small and therefore, it remains to be further determined whether the present results are able to be widely applied to patients with TSC-RAML. Due to the rarity of TSC-RAML, studies with large sample sizes are difficult to perform. In addition, the relatively small sample size may have introduced selection bias and affected the validity of the present results. Furthermore, the fact that the present study is a single-center study without external validation may be another limitation. Therefore, our group has started enrolling patients with TSC-RAML from different centers to validate the present findings in external cohorts. In the end, although the present results revealed the unique tumor microenvironment of TSC-RAML, further *in vitro* and *in vivo* experiments are required to elucidate the internal mechanism.

To conclude, the present results suggested that plasma proteins such as CCL5 and MMP9 may be useful diagnostic markers and disease burden markers. The unique inflammatory tumor microenvironment, particularly the monocyte-macrophages, also potentially has a crucial role in the development of TSC-RAML. Targeting the plasma diagnostic markers and inflammatory cells within the tumor microenvironment may be another breakthrough in TSC-RAML treatment.

Acknowledgements

Not applicable.

Funding

Not applicable.

Availability of data and materials

The RNA sequencing matrix may be obtained from Table SI and the raw data are being deposited in the Genome Sequence Archive (https://ngdc.cncb.ac.cn/bioproject/) under the accession number 'PRJCA011152'.

Authors' contributions

YuZ and LJ conceived the project and organized all the experiments. ZW and XL conducted the experiments and wrote the original manuscript. WW, YaZ, XW, ZL and YL collected the biological samples and clinical information and interpreted the data. JW, SS, JX, HS, YY and WS analyzed the data. All the authors have read and approved the manuscript. ZW and YuZ checked and confirmed the authenticity of the raw data.

Ethics approval and consent to participate

The study was performed in accordance with the Declaration of Helsinki and was approved by the Institutional Review Board of Peking Union Medical College Hospital and the Institute of Basic Medical Sciences, Chinese Academy of Medical Sciences (Beijing, China; approval no. KS2020127). Written informed consent was obtained from each patient for the use of their biological samples for scientific research and publication of all the related data.

Patient consent for publication

Not applicable.

Competing interests

The authors declare that they have no competing interests.

References

1. Curatolo P, Bombardieri R and Jozwiak S: Tuberous sclerosis. Lancet 372: 657-668, 2008.
2. Henske EP, Jóźwiak S, Kingswood JC, Sampson JR and Thiele EA: Tuberous sclerosis complex. Nat Rev Dis Primers 2: 16035, 2016.
3. Rebaine Y, Nasser M, Girerd B, Leroux C and Cottin V: Tuberous sclerosis complex for the pulmonologist. Eur Respir Rev 30: 200348, 2021.
4. Crino PB, Nathanson KL and Henske EP: The tuberous sclerosis complex. N Eng J Med 355: 1345-1356, 2006.
5. Amin S, Lux A, Calder N, Laugharne M, Osborne J and O'callaghan F: Causes of mortality in individuals with tuberous sclerosis complex. Dev Med Child Neurol 59: 612-617, 2017.
6. Shepherd CW, Gomez MR, Lie JT and Crowson CS: Causes of death in patients with tuberous sclerosis. Mayo Clin Proc 66: 792-796, 1991.
7. Saffari A, Brösse I, Wiemer-Kruel A, Wilken B, Kreuzaler P, Hahn A, Bernhard MK, van Tilburg CM, Hoffmann GF, Gorenflo M, *et al*: Safety and efficacy of mTOR inhibitor treatment in patients with tuberous sclerosis complex under 2 years of age-a multicenter retrospective study. Orphanet J Rare Dis 14: 96, 2019.
8. Bissler JJ, Kingswood JC, Radzikowska E, Zonnenberg BA, Frost M, Belousova E, Sauter M, Nonomura N, Brakemeier S, de Vries PJ, *et al*: Everolimus for angiomyolipoma associated with tuberous sclerosis complex or sporadic lymphangioleiomyomatosis (EXIST-2): A multicentre, randomised, double-blind, placebo-controlled trial. Lancet 381: 817-824, 2013.
9. Hatano T and Egawa S: Renal angiomyolipoma with tuberous sclerosis complex: How it differs from sporadic angiomyolipoma in both management and care. Asian J Surg 43: 967-972, 2020.
10. Northrup H and Krueger DA; International Tuberous Sclerosis Complex Consensus Group: Tuberous sclerosis complex diagnostic criteria update: Recommendations of the 2012 iinternational tuberous sclerosis complex consensus conference. Pediatr Neurol 49: 243-254, 2013.
11. Eijkemans MJ, van der Wal W, Reijnders LJ, Roes KC, van Waalwijk van Doorn-Khosrovani SB, Pelletier C, Magestro M and Zonnenberg B: Long-term follow-up assessing renal angiomyolipoma treatment patterns, morbidity, and mortality: An observational study in tuberous sclerosis complex patients in the Netherlands. Am J Kidney Dis 66: 638-645, 2015.

12. Gao F, Kataoka M, Liu N, Liang T, Huang ZP, Gu F, Ding J, Liu J, Zhang F, Ma Q, *et al*: Therapeutic role of miR-19a/19b in cardiac regeneration and protection from myocardial infarction. Nat Commun 10: 1802, 2019.
13. Guo M, Yu JJ, Perl AK, Wikenheiser-Brokamp KA, Riccetti M, Zhang EY, Sudha P, Adam M, Potter A, Kopras EJ, *et al*: Single-cell transcriptomic analysis identifies a unique pulmonary lymphangioleiomyomatosis cell. Am J Respir Crit Care Med 202: 1373-1387, 2020.
14. Hao Y, Hao S, Andersen-Nissen E, Mauck WM III, Zheng S, Butler A, Lee MJ, Wilk AJ, Darby C, Zager M, *et al*: Integrated analysis of multimodal single-cell data. Cell 184: 3573-3587.e29, 2021.
15. Stuart T, Butler A, Hoffman P, Hafemeister C, Papalexi E, Mauck WM III, Hao Y, Stoeckius M, Smibert P and Satija R: Comprehensive integration of single-cell data. Cell 177: 1888-1902.e21, 2019.
16. Aran D, Looney AP, Liu L, Wu E, Fong V, Hsu A, Chak S, Naikawadi RP, Wolters PJ, Abate AR, *et al*: Reference-based analysis of lung single-cell sequencing reveals a transitional profibrotic macrophage. Nat Immunol 20: 163-172, 2019.
17. Yu G, Wang LG, Han Y and He QY: clusterProfiler: An R package for comparing biological themes among gene clusters. OMICS 16: 284-287, 2012.
18. Wu T, Hu E, Xu S, Chen M, Guo P, Dai Z, Feng T, Zhou L, Tang W, Zhan L, *et al*: clusterProfiler 4.0: A universal enrichment tool for interpreting omics data. Innovation (Camb) 2: 100141, 2021.
19. Trapnell C, Cacchiarelli D, Grimsby J, Pokharel P, Li S, Morse M, Lennon NJ, Livak KJ, Mikkelsen TS amd Rinn JL: The dynamics and regulators of cell fate decisions are revealed by pseudotemporal ordering of single cells. Nat Biotechnol 32: 381-386, 2014.
20. Langfelder P and Horvath S: WGCNA: An R package for weighted correlation network analysis. BMC Bioinformatics 9: 559, 2008.
21. Langfelder P and Horvath S: Fast R functions for robust correlations and hierarchical clustering. J Statis Softw 46: i11, 2012.
22. Becht E, Giraldo NA, Lacroix L, Buttard B, Elarouci N, Petitprez F, Selves J, Laurent-Puig P, Sautès-Fridman C, Fridman WH and de Reyniès A: Estimating the population abundance of tissue-infiltrating immune and stromal cell populations using gene expression. Genome Biol 17: 218, 2016.
23. Bongaarts A, de Jong JM, Broekaart DW, van Scheppingen J, Anink JJ, Mijnsbergen C, Jansen FE, Spliet WG, den Dunnen WFA, Gruber VE, *et al*: Dysregulation of the MMP/TIMP proteolytic system in subependymal giant cell astrocytomas in patients with tuberous sclerosis complex: Modulation of MMP by MicroRNA-320d in vitro. J Neuropathol Exp Neurol 79: 777-790, 2020.
24. Broekaart DW, van Scheppingen J, Anink JJ, Wierts L, van Het Hof B, Jansen FE, Spliet WG, van Rijen PC, Kamphuis WW, de Vries HE, *et al*: Increased matrix metalloproteinases expression in tuberous sclerosis complex: Modulation by microRNA 146a and 147b in vitro. Neuropathol Appl Neurobiol 46: 142-159, 2020.
25. Zeng Z, Lan T, Wei Y and Wei X: CCL5/CCR5 axis in human diseases and related treatments. Genes Dis 9: 12-27, 2022.
26. McCormack FX, Inoue Y, Moss J, Singer LG, Strange C, Nakata K, Barker AF, Chapman JT, Brantly ML, Stocks JM, *et al*: Efficacy and safety of sirolimus in lymphangioleiomyomatosis. N Eng J Med 364: 1595-1606, 2011.
27. Muto Y, Sasaki H, Sumitomo M, Inagaki H, Kato M, Kato T, Miyai S, Kurahashi H and Shiroki R: Genotype-phenotype correlation of renal lesions in the tuberous sclerosis complex. Hum Genome Var 9: 5, 2022.
28. Zhang N, Wang X, Tang Z, Qiu X, Guo Z, Huang D, Xiong H and Guo Q: The correlation between tuberous sclerosis complex genotype and renal angiomyolipoma phenotype. Front Genet 11: 575750, 2021.
29. Cheng JB, Sedgewick AJ, Finnegan AI, Harirchian P, Lee J, Kwon S, Fassett MS, Golovato J, Gray M, Ghadially R, *et al*: Transcriptional programming of normal and inflamed human epidermis at single-cell resolution. Cell Rep 25: 871-883, 2018.
30. Holzinger D, Foell D and Kessel C: The role of S100 proteins in the pathogenesis and monitoring of autoinflammatory diseases. Mol Cell Pediatr 5: 7, 2018.
31. Pruenster M, Vogl T, Roth J and Sperandio M: S100A8/A9: From basic science to clinical application. Pharmacol Ther 167: 120-131, 2016.
32. Spiekerkoetter E, Guignabert C, de Jesus Perez V, Alastalo TP, Powers JM, Wang L, Lawrie A, Ambartsumian N, Schmidt AM, Berryman M, *et al*: S100A4 and bone morphogenetic protein-2 codependently induce vascular smooth muscle cell migration via phospho-extracellular signal-regulated kinase and chloride intracellular channel 4. Circ Res 105: 639-647, 2009.
33. Lam HC, Siroky BJ and Henske EP: Renal disease in tuberous sclerosis complex: Pathogenesis and therapy. Nat Rev Nephrol 14: 704-716, 2018.
34. Mootha VK, Lindgren CM, Eriksson KF, Subramanian A, Sihag S, Lehar J, Puigserver P, Carlsson E, Ridderstråle M, Laurila E, *et al*: PGC-1α-responsive genes involved in oxidative phosphorylation are coordinately downregulated in human diabetes. Nat Genet 34: 267-273, 2003.
35. Subramanian A, Tamayo P, Mootha VK, Mukherjee S, Ebert BL, Gillette MA, Paulovich A, Pomeroy SL, Golub TR, Lander ES and Mesirov JP: Gene set enrichment analysis: A knowledge-based approach for interpreting genome-wide expression profiles. Proc Natl Acad Sci USA 102: 15545-15550, 2005.
36. Ng HY, Oliver BG, Burgess JK, Krymskaya VP, Black JL and Moir LM: Doxycycline reduces the migration of tuberous sclerosis complex-2 null cells-effects on RhoA-GTPase and focal adhesion kinase. J Cell Mol Med 19: 2633-2646, 2015.
37. Pollizzi K, Malinowska-Kolodziej I, Doughty C, Betz C, Ma J, Goto J and Kwiatkowski DJ: A hypomorphic allele of Tsc2 highlights the role of TSC1/TSC2 in signaling to AKT and models mild human TSC2 alleles. Hum Mol Genet 18: 2378-2387, 2009.
38. Terraneo S, Lesma E, Ancona S, Imeri G, Palumbo G, Torre O, Giuliani L, Centanni S, Peron A, Tresoldi S, *et al*: Exploring the role of matrix metalloproteinases as biomarkers in sporadic lymphangioleiomyomatosis and tuberous sclerosis complex. A pilot study. Front Med (Lausanne) 8: 605909, 2021.
39. Li S, Yu S, Zhang C, Shu H, Liu S, An N, Yang M, Yin Q and Yang H: Increased expression of matrix metalloproteinase 9 in cortical lesions from patients with focal cortical dysplasia type IIb and tuberous sclerosis complex. Brain Res 1453: 46-55, 2012.
40. Ancona S, Orpianesi E, Bernardelli C, Chiaramonte E, Chiaramonte R, Terraneo S, Di Marco F and Lesma E: Differential modulation of matrix metalloproteinases-2 and -7 in LAM/TSC cells. Biomedicines 9: 1760, 2021.
41. Tyryshkin A, Bhattacharya A and Eissa NT: SRC kinase is a novel therapeutic target in lymphangioleiomyomatosis. Cancer Res 74: 1996-2005, 2014.
42. William M, Leroux LP, Chaparro V, Graber TE, Alain T and Jaramillo M: Translational repression of Ccl5 and Cxcl10 by 4E-BP1 and 4E-BP2 restrains the ability of mouse macrophages to induce migration of activated T cells. Eur J Immunol 49: 1200-1212, 2019.
43. Walens A, DiMarco AV, Lupo R, Kroger BR, Damrauer JS and Alvarez JV: CCL5 promotes breast cancer recurrence through macrophage recruitment in residual tumors. eLife 8: e43653, 2019.
44. Soria G and Ben-Baruch A: The inflammatory chemokines CCL2 and CCL5 in breast cancer. Cancer Lett 267: 271-285, 2008.
45. Rabe DC, Walker ND, Rustandy FD, Wallace J, Lee J, Stott SL and Rosner MR: Tumor extracellular vesicles regulate macrophage-driven metastasis through CCL5. Cancers (Basel) 13: 3459, 2021.
46. Farach LS, Pearson DA, Woodhouse JP, Schraw JM, Sahin M, Krueger DA, Wu JY, Bebin EM, Lupo PJ, Au KS, *et al*: Tuberous sclerosis complex genotypes and developmental phenotype. Pediatr Neurol 96: 58-63, 2019.
47. Ogórek B, Hamieh L, Hulshof HM, Lasseter K, Klonowska K, Kuijf H, Moavero R, Hertzberg C, Weschke B, Riney K, *et al*: TSC2 pathogenic variants are predictive of severe clinical manifestations in TSC infants: Results of the EPISTOP study. Genet Med 22: 1489-1497, 2020.
48. Bottolo L, Miller S and Johnson SR: Sphingolipid, fatty acid and phospholipid metabolites are associated with disease severity and mTOR inhibition in lymphangioleiomyomatosis. Thorax 75: 679-688, 2020.
49. Feng Y, Mischler WJ, Gurung AC, Kavanagh TR, Androsov G, Sadow PM, Herbert ZT and Priolo C: Therapeutic targeting of the secreted lysophospholipase D autotaxin suppresses tuberous sclerosis complex-associated tumorigenesis. Cancer Res 80: 2751-2763, 2020.

50. Li S, Thangapazham RL, Wang JA, Rajesh S, Kao TC, Sperling L, Moss J and Darling TN: Human TSC2-null fibroblast-like cells induce hair follicle neogenesis and hamartoma morphogenesis. Nat Commun 2: 235, 2011.
51. García-Aguilar A, Guillén C, Nellist M, Bartolomé A and Benito M: TSC2 N-terminal lysine acetylation status affects to its stability modulating mTORC1 signaling and autophagy. Biochim Biophys Acta 1863: 2658-2667, 2016.
52. Wu Z, Wu H, Md S, Yu G, Habib SL, Li B and Li J: Tsc1 ablation in Prx1 and Osterix lineages causes renal cystogenesis in mouse. Sci Rep 9: 837, 2019.
53. Wu K, Lin K, Li X, Yuan X, Xu P, Ni P and Xu D: Redefining tumor-associated macrophage subpopulations and functions in the tumor microenvironment. Front Immunol 11: 1731, 2020.
54. Li S, Takeuchi F, Wang JA, Fuller C, Pacheco-Rodriguez G, Moss J and Darling TN: MCP-1 overexpressed in tuberous sclerosis lesions acts as a paracrine factor for tumor development. J Exp Med 202: 617-624, 2005.
55. Byles V, Covarrubias AJ, Ben-Sahra I, Lamming DW, Sabatini DM, Manning BD and Horng T: The TSC-mTOR pathway regulates macrophage polarization. Nat Commun 4: 2834, 2013.